Wendelstein 7-X on the path to long-pulse high-performance operation

M. Endler[1], J. Baldzuhn[1], C. D. Beidler[1], H.-S. Bosch[1], S. Bozhenkov[1], B. Buttenschön[1], A. Dinklage[1], J. Fellinger[1], Y. Feng[1], G. Fuchert[1], Y. Gao[1], J. Geiger[1], O. Grulke[1], D. Hartmann[1], M. Jakubowski[1], R. König[1], H. P. Laqua[1], S. Lazerson[1], P. McNeely[1], D. Naujoks[1], U. Neuner[1], M. Otte[1], E. Pasch[1], T. Sunn Pedersen[1], V. Perseo[1], A. Puig Sitjes[1], K. Rahbarnia[1], N. Rust[1], O. Schmitz[2], A. Spring[1], T. Stange[1], A. von Stechow[1], Y. Turkin[1], E. Wang[3], R. C. Wolf[1], and the W7-X Team*

[1]*Max-Planck-Institut für Plasmaphysik, 17491 Greifswald, Germany*

[2]*University of Wisconsin, Madison, WI, USA*

[3]*Forschungszentrum Jülich GmbH, Institut für Energie- und Klimaforschung — Plasmaphysik, Partner of the Trilateral Euregio Cluster (TEC), Jülich, Germany*

8th March 2021

Abstract

The Wendelstein 7-X project is aimed at demonstrating that an optimised stellarator is an attractive candidate for a fusion reactor. This requires the achievement of a number of technical and physics goals. Several of these goals have already been achieved in the first three experimental campaigns. We shall exemplify this by a number of results. One important goal is the demonstration of quasi-steady-state operation at high plasma density and temperature for half an hour, which encompasses the physical and technical requirements of stable operation with density and impurity control, cw heating, water-cooled targets, particle exhaust, and an appropriate control and data acquisition system for long-pulse operation. In the previous

*see [1] for the members of the W7-X Team

experimental campaigns, with uncooled targets, stationary discharges for up to 25 s with 5 MW heating power and up to 100 s with 2 MW heating power were achieved. For the next operational phase, to start in 2022, water-cooled targets are being installed, water cooling will be provided for all first-wall components, and a number of further upgrades to plasma heating, vacuum and fuelling systems as well as diagnostics will become available. With this equipment, the further goals of the project will be tackled, including the stepwise extension of discharge intervals to the multi-minute range. The experimental results so far have confirmed the neoclassical theory underlying several of the optimisation goals. At the same time, they showed that an optimisation is also required with respect to anomalous transport. In the future operational phases we aim at building a solid theoretical, experimental and technical foundation for the design of a next-step stellarator device.

1 Goals of the Wendelstein 7-X project

Wendelstein 7-X (W7-X) was designed and built to demonstrate that an optimised stellarator is an attractive candidate for a fusion reactor. Before, it had been established in neoclassical theory that the energy transport in a classical stellarator would be very large under reactor-relevant plasma conditions (i. e., in the long-mean-free-path regime) [2], forcing such a reactor to an uneconomically large size. This is due to the loss of toroidal symmetry in contrast to a tokamak configuration. However, quasi-symmetric magnetic configurations can be designed in which the neoclassical transport is reduced to a tolerable level [3].

To demonstrate the reactor capability of an optimised stellarator, goals were defined for the W7-X project [4], both for physics results and for technical achievements. The physics goals are

- the demonstration of a reactor-relevant plasma parameter regime with ion temperatures above 5 keV and densities above $10^{20}\,\mathrm{m}^{-3}$,
- the demonstration of magnetohydrodynamic (MHD) stability at $\langle\beta\rangle = 5\,\%$,
- a sufficiently high energy confinement time (i. e., similar as in a tokamak of comparable size) for thermal particles, and
- a sufficiently good confinement of highly energetic ions, relevant for the α particles from fusion reactions.

The technical goals are

- steady-state operation of a magnetic field generated by modular superconducting coils, with low error fields,

- control of plasma density and impurity content and, based on these prerequisites,
- to achieve quasi-steady-state operation in a reactor-relevant parameter regime.

Since the physics goals governed most of the optimisation criteria, their achievement would confirm the models on which the optimisation is based and would qualify their use for the design of a stellarator reactor.

The first technical goal, including the demonstration that the construction of non-planar superconducting coils is feasible, was already achieved during commissioning of the magnet system [5]. The criterion of low error fields will be discussed and quantified in section 4.1. The second technical goal is closely related to the operation of the divertor, which determines power and particle exhaust. At the same time, the achievement of the second technical goal is a fundamental prerequisite for the third technical goal, the quasi-steady-state operation in a reactor-relevant parameter regime.

After introducing the W7-X device, focusing on its magnet system, its plasma heating systems and its divertor in section 2, we shall summarise in section 3 the increasing technical capabilities within the three past operational phases (OPs) and within the next OP to come. In section 4, we shall show selected results from the past OPs demonstrating the achievement of several of the project goals, namely the quality of the magnetic field (section 4.1), the confirmation of low bootstrap current (section 4.2) and low neoclassical transport of thermal particles (section 4.3), and stationary operation at high plasma density, low impurity content and with divertor detachment for intervals as long as the uncooled targets and first wall permitted (section 4.5). We also discuss anomalous transport and progress in the understanding of turbulence in section 4.4. A brief outlook to the core device upgrades and several examples for diagnostic upgrades and new diagnostics, to several focal topics of the next operational campaign and to longer-term developments will be given in section 5. In section 6 we shall discuss the contributions of the W7-X project to the development of a fusion reactor and the place of W7-X in this development, before we conclude in section 7.

2 The W7-X device

2.1 Coil system and magnetic configurations

The principal coil system of W7-X consists of 70 superconducting coils. They are arranged in 5 identical modules, each of which is symmetric under a 180° rotation around a radial axis through its centre ("stellarator symmetry"). This makes up 10 so-called half modules with 5 different non-planar and 2 different planar coils each. The coils are attached to a central support ring. This entire magnet system is located in a cryostat, formed by the plasma vessel on the inside and an outer vessel on the outside of the coils (see fig. 1). For operation, the NbTi superconductor is cooled by liquid helium to a temperature of 4.5 K.

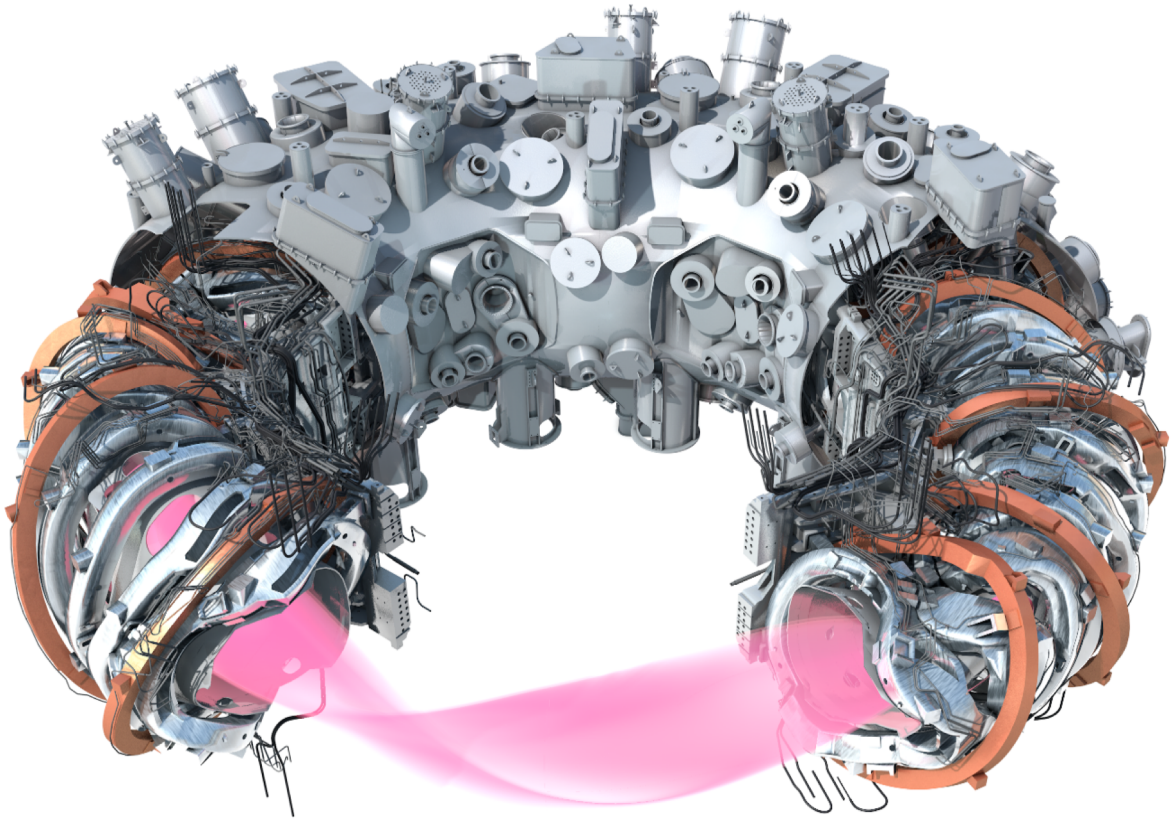

Figure 1: Plasma, superconducting coil system and cryostat of W7-X. The plasma shape is shown in transparent pink (see also fig. 2), the non-planar coils in grey, the planar coils in brown, the outer vessel of the cryostat in grey. 1/5 of the coil system and 3/5 of the outer vessel are blanked. The average major radius of the plasma axis is 5.5 m, the average minor radius of the plasma cross section is 0.5 m.

The theoretical concept behind the magnetic configurations of W7-X and the modular coil system is explained in [4], its technical realisation is highlighted in [6], and details about the design of the cryostat can be found in [7].

The 50 non-planar coils by themselves are sufficient to generate a confining magnetic field. The flux surfaces form a slender torus with an average major radius of 5.5 m and an average minor radius of 0.5 m (see fig. 2). Their cross section reflects the fivefold toroidal symmtery and the flip symmetry within each module, changing between bean-shaped and triangular as shown in the Poincaré plots in fig. 2.

The coil currents in the five different types of non-planar coil and two different types of planar coil can be controlled independently (within certain limits set by the electromagnetic forces acting on the coils). This results in a remarkable flexibility of magnetic configuration, offering the option to compare configurations with a different weighting of the various optimisation criteria of W7-X. The plasma shape and cross sections shown in

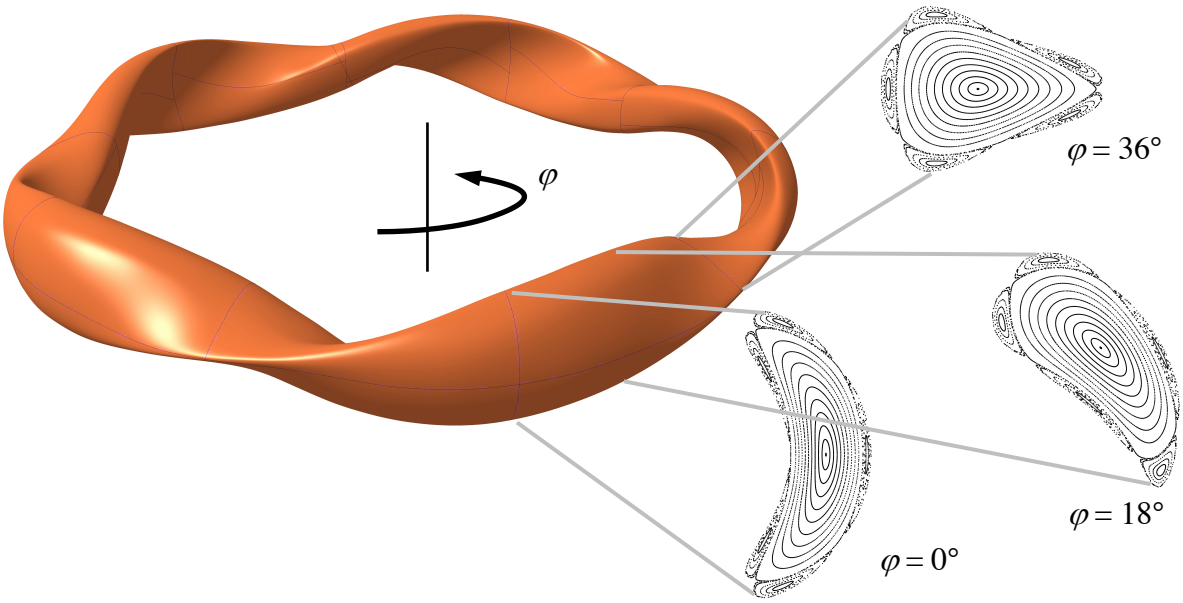

Figure 2: Shape of the Last Closed Flux Surface (LCFS) in W7-X "standard" magnetic configuration. In this configuration, $\iota = 1 = 5/5$ at the plasma edge, and the separatrix of five natural magnetic islands is therefore defining the LCFS. This can be seen in the Poincaré plots shown on the right for the bean-shaped ($\varphi = 0^o$), the $\varphi = 18^o$ and the triangular ($\varphi = 36^o$) cross section.

fig. 2 are those resulting if the current is equal in all non-planar coils and there is 0 current in the planar coils. This so-called "standard" configuration has a rotational transform $\iota = 1$ at the plasma edge. The rotational transform is the number of poloidal revolutions around the plasma column a field line takes per toroidal revolution, i. e., it is the inverse of the tokamak safety factor q. Islands occur naturally in these configurations for rational values $\iota = n/m$ with n being a multiple of the toroidal periodicity of 5. In the standard configuration, five islands are located at the $\iota = 1$ surface at the plasma edge. Use of these edge islands is made to operate the island divertor (see section 2.3).

With non-zero currents in the planar coils, the toroidal field component can be increased or reduced, thus modifying the rotational transform.

With different coil currents in the five non-planar coil types, the magnetic mirror between the bean-shaped and the triangular planes can be varied, thus changing the fraction and location of trapped particles. A quantity summarising the effect of the magnetic mirror on neoclassical transport is the effective helical ripple of the magnetic field, ε_{eff} (see, e. g., [8, 9, 10]). A low effective helical ripple is achieved in the "standard" and "low-mirror" configurations, which should yield low neoclassical transport for thermal particles (see section 4.3). In the "high-mirror" configuration, the toroidal plasma current (bootstrap current) should be smallest, and this configuration is also designed for good

confinement of fast ions at sufficiently high plasma pressure. In addition, the magnetic curvature varies between bean-shaped and triangular plane. Since its magnitude and sign has an impact on certain instability mechanisms, the fraction and location of trapped particles, and thus the magnetic mirror, may also have an impact on plasma turbulence.

Further use of the configuration space can be made to modify the target load and its location [11, 12].

The magnet system is completed by two sets of copper coils operated at room temperature (see fig. 3). Inside the plasma vessel, behind the baffles of each divertor unit,

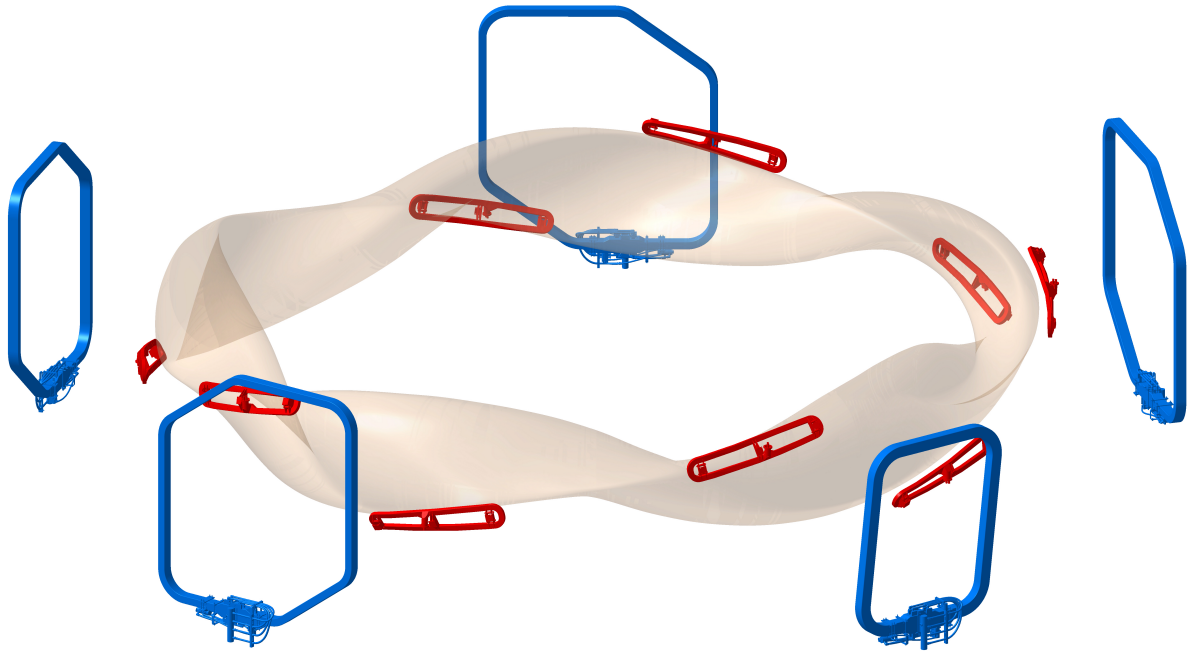

Figure 3: Arrangement of the island control coils (red) inside the plasma vessel and the trim coils (blue) outside the cryostat, shown together with the shape of the last closed flux surface (transparent beige) of the "standard" magnetic configuration.

there is an island control coil [13, 14, 15] to modify the size and, to some degree, the poloidal location of the edge magnetic islands. Outside the cryostat, there are five trim coils with individual power supplies to reduce leading error field components which might be caused by asymmetries of the coil system — or to generate such error fields to study their impact. The currents in the island control coils can also be adjusted individually to balance smaller but higher order (in terms of Fourier components) error fields.

2.2 Plasma heating systems

Three different heating systems have been planned for W7-X. The Electron Cyclotron Resonance Heating (ECRH) system is the workhorse of W7-X plasma heating [16]. Presently,

it is powered by 10 gyrotrons operating at 140 GHz (2nd harmonic of the electron cyclotron frequency at 2.5 T). The gyrotrons have a design output power of 1 MW in cw operation. Their guaranteed power at delivery was 0.9 MW, the prototype and a further gyrotron have lower power. After transmission losses, a total absorbed power of up to 7.5 MW has been available in the plasma from this system. ECRH is routinely used to start up the plasma in the beginning of a discharge. It can also be used to drive a toroidal current in different radial locations (Electron Cyclotron Current Drive — ECCD, see section 4.2).

The second heating system is Neutral Beam Injection (NBI). Space is available for up to 8 ion sources in two injector boxes [17, 18]. The first two ion sources have been available during the last operational phase of W7-X with a total of 3 MW of hydrogen neutrals injected into the plasma in pulses of up to 5 s. The neutral beams are injected with a velocity component parallel to the magnetic field direction, and therefore current drive is possible by asymmetric use of the ion sources [19].

The third system is Ion Cyclotron Resonance Heating (ICRH) [20, 21], which will become available in the next operational phase (see section 3).

An important purpose of NBI and ICRH, besides heating the bulk plasma, is the generation of fast ions. As stated in section 1, one of the optimisation goals of W7-X is a good confinement of fast ions: hydrogen ions of the order of 50–100 keV in W7-X will have a similar proportion of their gyroradius to the minor radius of the device as fusion alpha particles in a stellarator reactor of this type, taking into account the size scaling between these devices. They will therefore also have similar collisionless loss times. In both cases, the influence of the neoclassical electric field on their confinement will be negligible [22], such that the behaviour of such fast ions in W7-X is a good test of this optimisation.

2.3 Divertor

In the usual divertor tokamak, a magnetic separatrix is generated by the plasma current and the currents in the divertor coils. This separatrix and its X-point(s) are toroidally symmetric. In non-axisymmetric magnetic configurations, magnetic islands can occur where the rotational transform ι assumes rational values, even without plasma currents. These islands, their O-points and the X-points of their separatrix revolve helically around the plasma column according to the local value of the rotational transform (see fig. 4). They can be used to build an island divertor. A comparison between an island divertor and the poloidal divertor of a tokamak can be found in [23]. The differences and the location of target plates is well illustrated in fig. 1 of that publication.

If we consider individual field lines within an island and trace them toroidally, they revolve together with the island around the plasma axis. However, the revolution of a field line *within the island around the "island axis", i. e., the O-point,* takes many toroidal revolutions. This is illustrated in fig. 5 for the W7-X "standard" configuration. If an island is intersected by a target plate, it takes order of 5 toroidal revolutions before a field

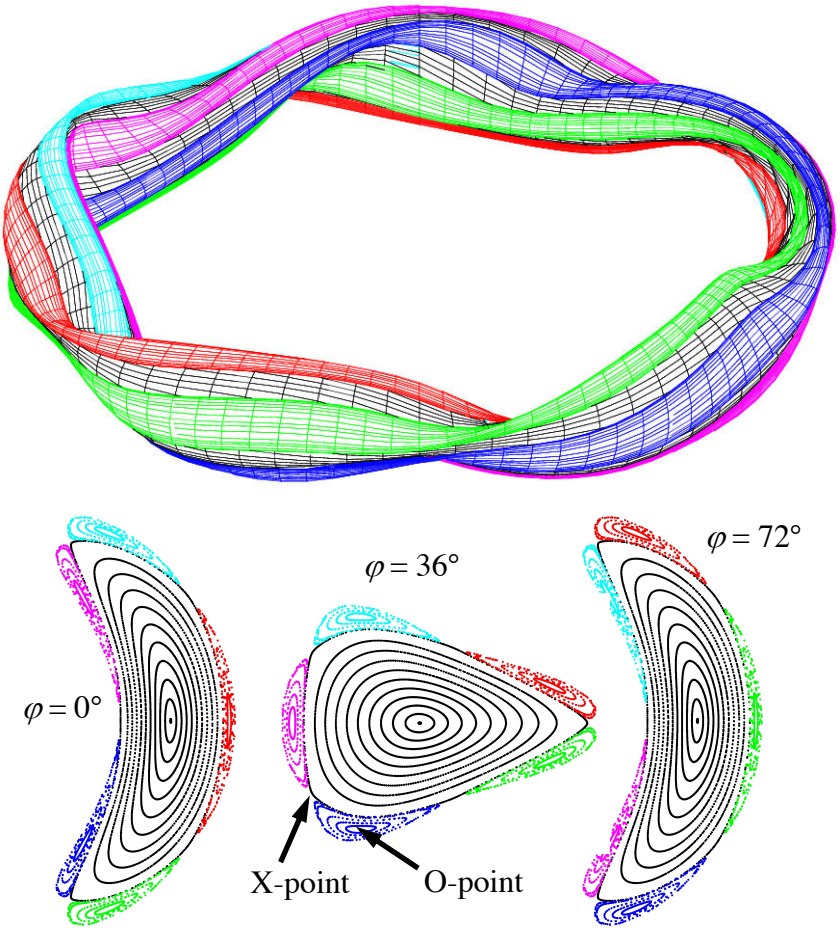

Figure 4: The five edge islands of the "standard" magnetic configuration are here represented in different colours to clarify their rotation around the plasma axis. The locations of one X-point and one O-point of the island separatrix are indicated.

line starting close to the LCFS intersects the target plate. Since one toroidal revolution corresponds to $\sim 35\,\mathrm{m}$ in W7-X, connection lengths between targets of $\sim 300\,\mathrm{m}$ are typical within the islands close to the separatrix. This favours a widening of the power-carrying layer within the islands and thus a broadening of the strike lines on the target plates [24, 23, 25].

Once plasma has been transported across the separatrix into an island, it will predominantly flow parallel to the magnetic field toward the nearest target plate. This implies a stagnation point of the parallel flow velocity and opposite toroidal velocity components on the poloidally opposing sides of an island (compare fig. 5). This is indeed well visible in the data of the Coherence Imaging Spectroscopy (CIS) diagnostic measuring the Doppler shift of impurity ions [26], which in this case are dragged along with the bulk plasma flow.

Since the islands are arranged helically around the plasma axis, and the shape of the

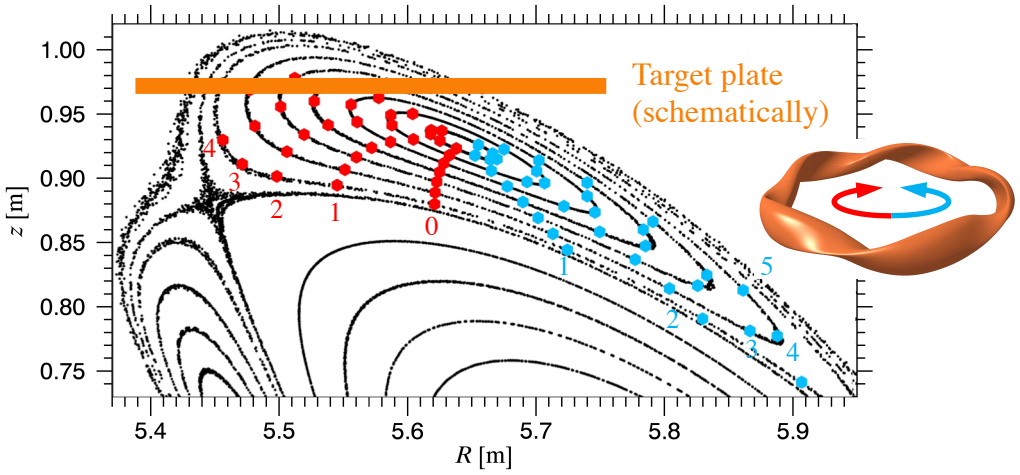

Figure 5: Penetration points of field lines on island flux surfaces (detail of Poincaré plot of bean-shaped plane in fig. 2, "standard" magnetic configuration). If tracing is started in the red points of the central row in the direction marked in red for four toroidal revolutions, the remaining red penetration points will result (marked 1–4 for one flux surface). Likewise, the penetration points marked in blue result from tracing for five toroidal revolutions in the opposite direction (marked 1–5). A possible location of a target plate is indicated. The revolution of the field lines around the O-line of the island is very slow, i. e., the parallel connection length from the stagnation point close to the LCFS to the intersection with the target is typically of order 150 m.

plasma cross-section changes for different toroidal positions, not every location is equally well suited to place target plates. In practice, 10 separate Divertor Units (DUs) are placed in equivalent positions, following the plasma symmetry (see fig. 6). Each of the DUs has a long horizontal target and a shorter vertical target with a pumping gap in between to allow neutral particles to escape into the sub-divertor space, where they can be pumped. Additional baffles are placed adjacent to the target plates to prevent the neutral gas from streaming back to the main chamber in unfavourable locations. The targets are three-dimensionally shaped in such a way that the thermal load does not exceed the design value of $10\,\mathrm{MW/m^2}$ locally (technological limit for the water-cooled target elements). The resulting targets intersect the magnetic field at angles of 1°–3° in those regions where the heat flux along the magnetic field is largest, thus limiting the thermal load to the targets as required. Whereas so far DUs with uncooled graphite targets [27] have been used, new DUs with water-cooled Carbon-Fibre reinforced Carbon (CFC) targets of identical surface shape [28] are presently being installed.

The shape of the targets is a compromise to allow divertor operation in different magnetic configurations. In any one configuration, only a small fraction of the target surface is hit by the strike line (see fig. 7). In a reactor, designed to operate in one specific

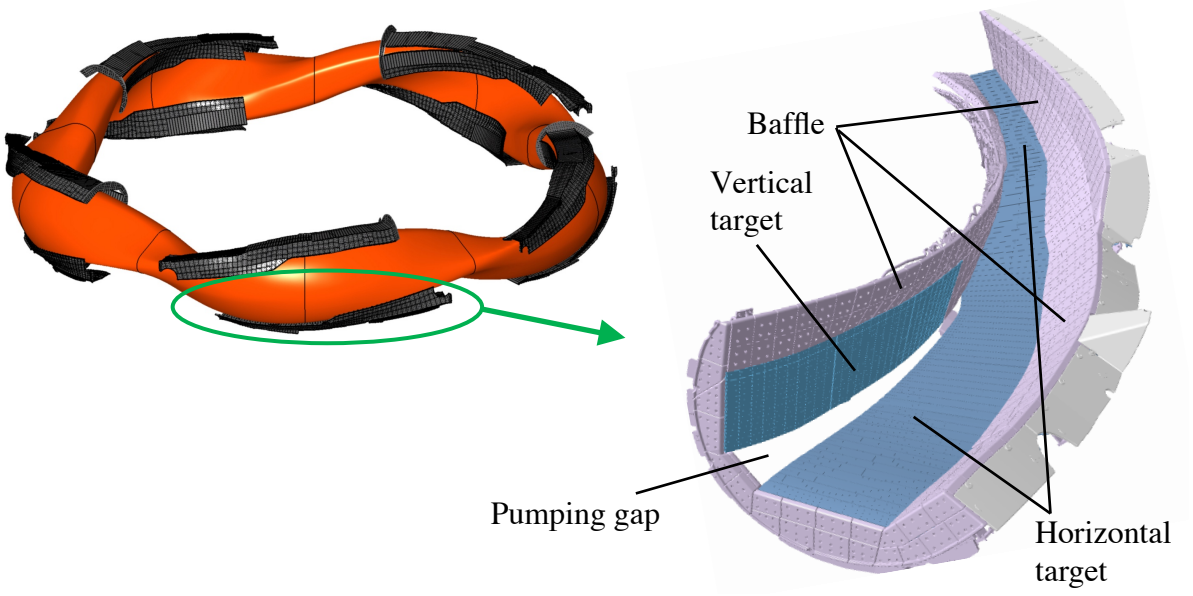

Figure 6: Arrangement of the ten divertor units together with the last closed flux surface of the W7-X "standard" configuration (left). A single divertor unit (DU) consists of a toroidally extended horizontal target and a shorter vertical target with a pumping gap in between. In different magnetic configurations, the main heat flux loads different parts of the target surface (see fig. 7). The baffles prevent neutral gas from flowing back into the main plasma from the volume behind the targets.

magnetic configuration, the target shape could be optimised to increase the surface area with high heat load and thus to more uniformly distribute the power density to the target surface.

3 Operational phases of W7-X

So far, there were three Operational Phases (OPs) of W7-X, each comprising several months of plasma operation. They were called OP1.1, OP1.2a and OP1.2b.

In OP1.1, no graphite tiles to protect the first wall and no divertor units were installed. Instead, five uncooled graphite limiters on the torus inboard side defined the LCFS. Correspondingly, the heating energy was limited to 4 MJ per discharge to avoid any damage to the unprotected in-vessel components. Summaries of the OP1.1 achievements can be found in [30, 31, 32].

For OP1.2, graphite tiles were installed on a large fraction of the first wall. The limiters of OP1.1 were removed and uncooled divertor units with graphite targets and baffles were installed instead (see section 2.3), forming the so-called Test Divertor Unit (TDU). This allowed to raise the discharge energy limit to 80 MJ (for the last discharges

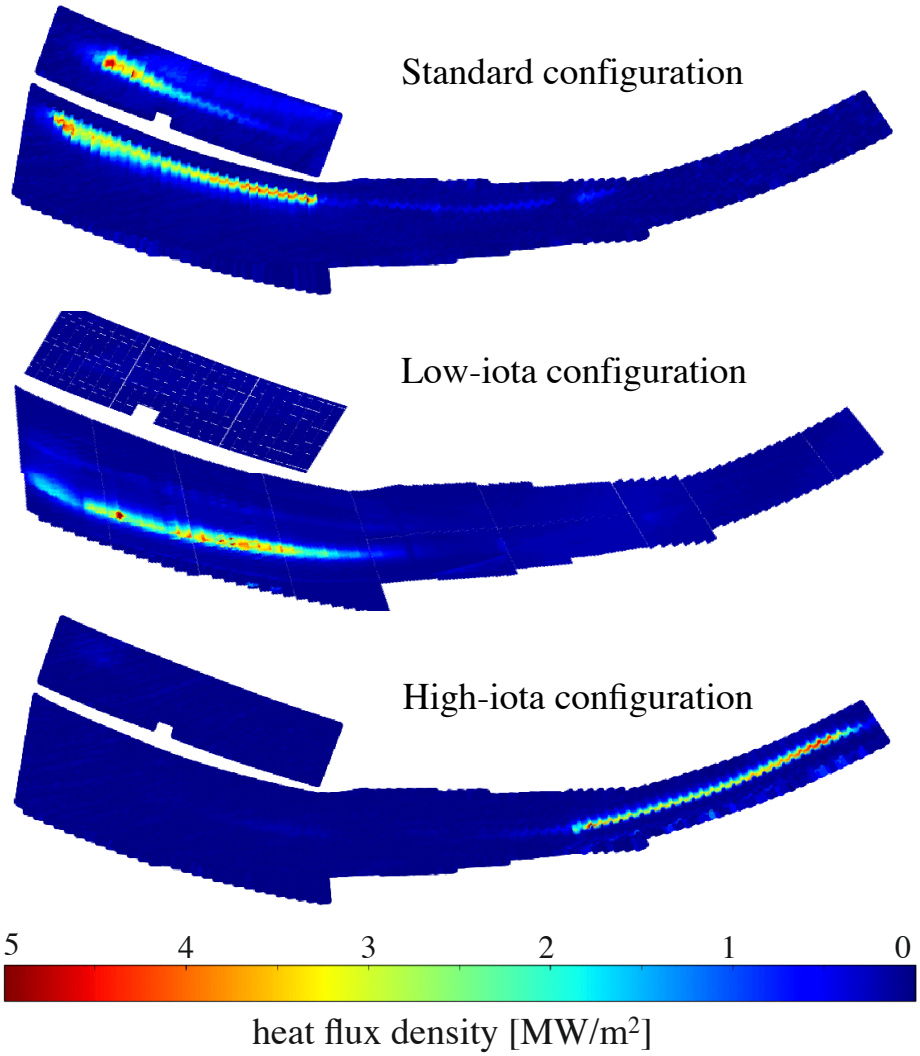

Figure 7: Heat flux patterns to the targets of one divertor unit for magnetic configurations with different edge rotational transform, calculated from infrared data [29]. Only a small fraction of the target surface is loaded in any single configuration, but the design is capable to provide divertor action for a variety of different configurations, including configurations with volume-averaged β up to 5 %.

of OP1.2b, it was permitted to stepwise exceed this limit, see section 4.5).

In OP1.2a, the maximum heating power available in the plasma was 7.5 MW ECRH. A hydrogen pellet injector was in use which could deliver up to $\sim$40 pellets per discharge [33].

The split between OP1.2a and OP1.2b served to install two so-called scraper elements to test a protection scheme for the divertor pumping gap (for details on these scraper elements, see [34]). In addition, two ion sources became available for NBI with 3 MW

absorbed power in the plasma, and boronisation of the in-vessel components could be performed for the first time, which dramatically extended the operating parameter range achievable (see section 4.5). The OP1.2 achievements are summarised in [35, 36, 1].

For the next operational phase, OP2, the uncooled TDU will be exchanged against water-cooled High Heat Flux (HHF) divertor units [28] of identical surface geometry (see section 2.3), and all further plasma facing components will be water-cooled. This should enable us to stepwise extend the discharge energy limit up to 18 GJ, which is set by the size of the cooling water basin, corresponding to a 10 MW half-hour operation. For ECRH it is planned to deliver 8.5 MW absorbed power in cw operation, NBI should deliver > 6 MW for pulses of at least 10 s, and ICRH should deliver > 1.5 MW for pulses of 10 s. Cryopumps are being installed behind the divertor targets [37], and a steady-state pellet injector of the same design as foreseen for ITER [38] will be installed. Further upgrades on a longer time scale will be discussed in section 5.3.

According to the present schedule, commissioning for OP2 should start in the beginning of 2022. Plasma operation is expected to follow at the end of 2022.

4 Selected results from the first three operation phases

4.1 Feasibility of superconducting coil system with non-planar coils and sufficiently small error field

One technical goal of the W7-X project was to demonstrate that it is possible to build a modular system of superconducting non-planar coils with sufficient accuracy. The error fields in a toroidal plasma confinement device are often expressed in terms of their Fourier components: For some flux surface, the component of the true magnetic field perpendicular to the ideal flux surface is Fourier transformed in poloidal and toroidal directions, resulting in components B_{nm}. The most critical types of error field are those with low-order Fourier components resonant with the $\iota = 1$ surface, i. e., B_{11}, B_{22}, B_{33} and B_{44} [39]. Fig. 8 shows the effect of a hypothetical B_{11} component of $B_{11}/B_0 = 2.7 \times 10^{-4}$ for the magnetic "standard" configuration: The separatrix common to all five islands in the unperturbed case (see fig. 4) splits, and one separatrix (cyan in fig. 8) encloses all five islands. In consequence, as field line diffusion calculations show, the heat flux to the targets becomes strongly asymmetric, loading two out of the ten DUs much stronger than the others.

To avoid a field error of this amplitude, a complete chain of geometric surveys was established, ranging from the manufacturing of the winding packs to the positioning of machine modules in their final location, including adaptation of the set coordinates to compensate the accumulated errors of previous assembly steps [40, 5]. Field errors of limited amplitude can be partly balanced by an asymmetric operation of the island

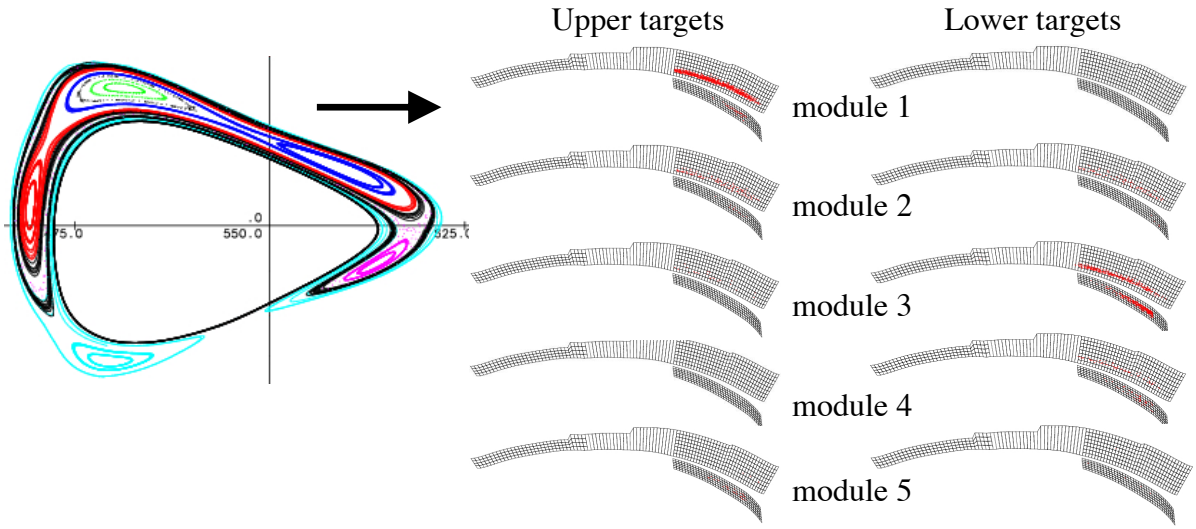

Figure 8: Left: Poincaré plot of the edge island topology generated by geometrical errors in the assembly of the magnet system (in this case: statistical tilting of entire machine modules by up to 0.1°, corresponding to 5 mm). An error field (1,1) Fourier component $B_{11}/B_0 \approx 2.7 \times 10^{-4}$ is thus generated. — Right: Modelling of the resulting power load distribution to the targets of the 10 divertor units by field line diffusion. Almost the entire power flows to only two divertor units.

control coils (see section 2.1). As an additional risk mitigation, the trim coils were added to the design, which can balance still larger B_{11} error field components.

The quality of the magnetic flux surfaces of the vacuum field was initially measured with electron guns and fluorescent rods [41, 42, 43, 44], and later the asymmetry of the heat loads to the limiters (in OP1.1) or to the divertor targets was derived from thermocouple measurements and infrared imaging [45, 46, 47, 48]. The asymmetry is quantified in fig. 9 by the relative standard deviation (standard deviation divided by average value) of the heat loads to the divertor units, separately for the five upper DUs and the five lower DUs. For totally symmetric loading, this would be 0. Fig. 9 shows the change in asymmetry which can be achieved by applying a sinusoidal spatial pattern of current to the five trim coils. A sharp minimum in the asymmetry is found for the spatial phase best balancing the error field. The remaining asymmetry could be further reduced by an asymmetric operation of the island control coils. The amplitudes of the error field components derived from flux surface measurements are $B_{11}/B_0 \approx 0.5 \times 10^{-4}$ and $B_{22}/B_0 \approx 0.6 \times 10^{-4}$ [48]. This is significantly smaller than assumed for the simulation shown in fig. 8. Hence, the trim coil current of $\sim 100\,\mathrm{A}$ used to minimise the error field is much smaller than the maximum capacity of the trim coils of 1.8 kA.

We therefore conclude that a modular system of superconducting non-planar coils can be built with sufficiently high accuracy.

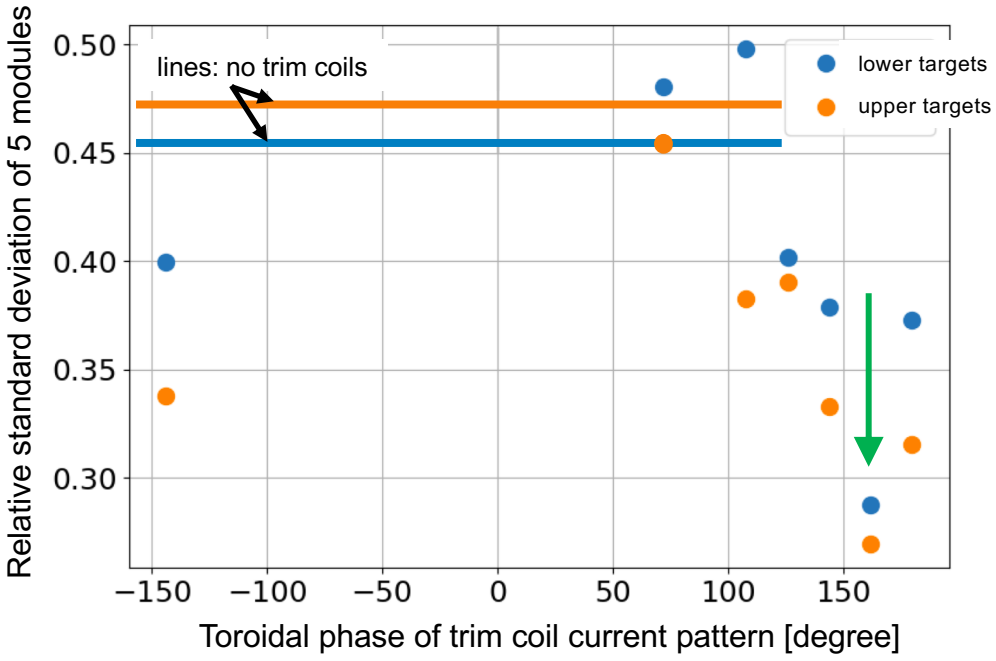

Figure 9: Asymmetry of heat loads to the targets in "standard" magnetic configuration, expressed as the standard deviation of the total heat fluxes per target, divided by the average of these heat fluxes. The analysis is separated for the five upper and the five lower DUs, in order not to mix the toroidal asymmetries with potential up-down asymmetries, which may have a different reason [49]. The five trim coils were operated in a spatial sine pattern with an amplitude of 100 A. The phase of this pattern around the torus was varied in different discharges, as shown on the abscissa, whereas the horizontal lines indicate the result with 0 trim coil current. The green arrow indicates the clear minimum of asymmetry. The phase at which this minimum is reached agrees well with the expectation for error field compensation as derived from flux surface measurements [48].

4.2 Optimisation for low bootstrap current

A toroidal current in stellarators has advantages and disadvantages. On the one hand side it can increase the rotational transform of the magnetic field (see section 2.1): The same value of the rotational transform can then be obtained with less twisted field coils, which can be an advantage for coil design and manufacturing. On the other side, the current can be a source of plasma instabilities. Furthermore, the operation of the island divertor is facilitated if the rotational transform and hence the radial location of the edge islands does not change much between vacuum field and equilibrium field with plasma. This is also an advantage in view of the long L/R times in W7-X plasmas of several 10 s (see, e. g., [10, 50, 1]). After plasma startup, the toroidal current will evolve toward its equilibrium value during such a long time interval (see fig. 10), implying a significant shift

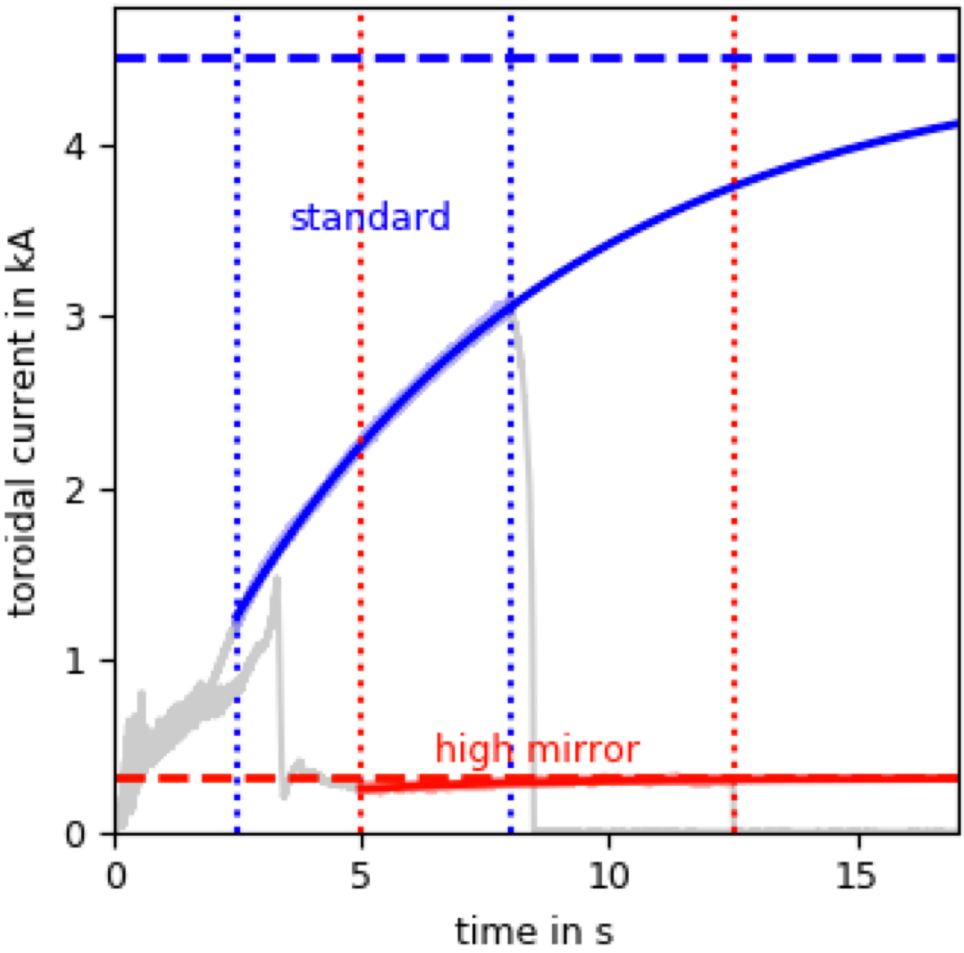

Figure 10: Examples for the evolving toroidal current in "standard" and "high-mirror" magnetic configurations. The current measured by a Rogowski coil is depicted in grey. Initially, the bootstrap current is shielded by plasma currents, which then exponentially decay on the L/R time scale. Fits (solid coloured lines) to the experimental time traces within the intervals marked by vertical dotted lines, modelling this decay, yield the asymptotic values of the current (dashed coloured lines), i. e., the bootstrap currents for the two configurations, which differ in their effective helical ripple $\varepsilon_{\mathrm{eff}}$. This quantity determines the fraction of trapped particles (see section 2.1). A higher $\varepsilon_{\mathrm{eff}}$ results in lower bootstrap current. Figure from [51].

of the strike line location [52, 53, 54]. It was therefore decided to include a low bootstrap current as one of the optimisation goals of W7-X.

In fig. 11, the experimentally determined equilibrium values of the bootstrap current are compared for different magnetic configurations with the values calculated by neoclassical theory [51]. In view of the very small currents in a device of this size and taking into account that these small values are the result of competing contributions with opposite

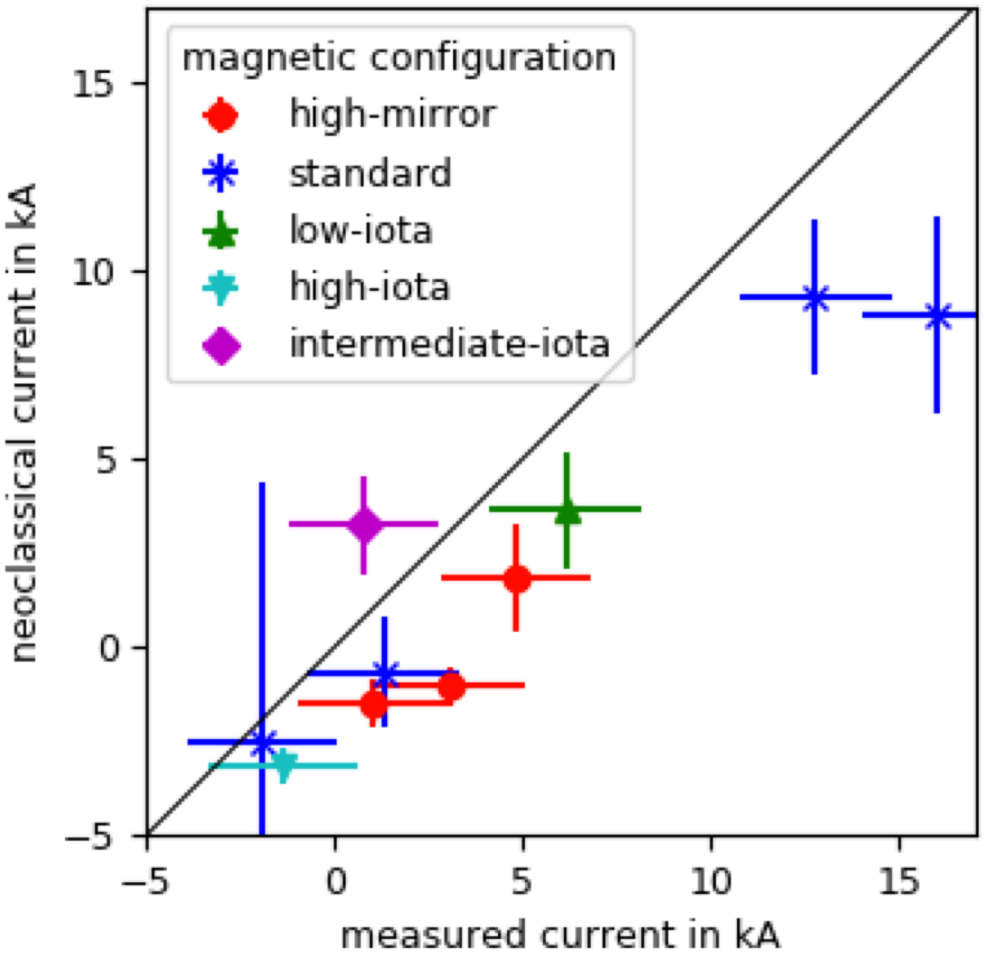

Figure 11: Comparison of the measured bootstrap current with the values calculated by neoclassical theory for different magnetic configurations. Figure from [51].

sign, the agreement is excellent.

One option to control the remaining toroidal current is ECCD. This is demonstrated by two examples, both aiming to avoid or reduce the impact of the transient current phase after plasma startup:

In fig. 12 we compare two discharges without and with ECCD. Without ECCD, the usual evolution of the toroidal current within the 25 s discharge interval is observed. With ECCD, the bootstrap current is compensated, and the observed toroidal current stays close to 0.

In our second example, the aim is to accelerate the evolution of the toroidal current by adding ECCD to the bootstrap current. Part of the launchers directing the ECR microwave beams into the plasma are in a position to drive a toroidal current whereas other launchers are in a position to drive no toroidal plasma current. Initially, ECCD in addition to the bootstrap current results in a faster increase of the total toroidal plasma

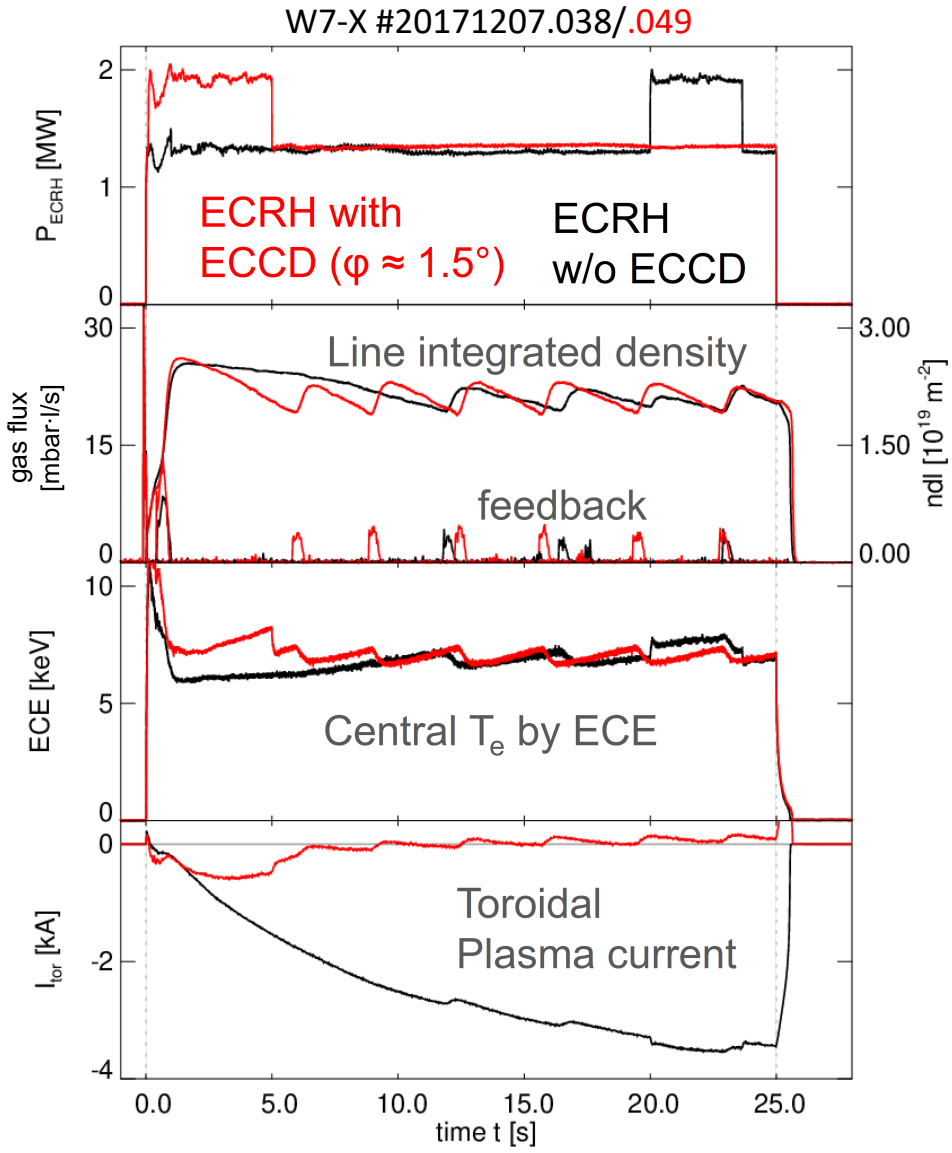

Figure 12: Comparison of a discharge without ECCD (black) and a discharge with ECCD to balance the bootstrap current (red). ECRH power was the same in both cases, plasma density and electron temperature are approximately equal in both discharges. For ECCD, the ECR beams were launched 1.5° out of the direction perpendicular to the magnetic field. Without ECCD, the usual evolution of the toroidal current is observed, whereas with ECCD, the total current stays stationary close to 0 during the entire discharge. Figure adapted from [55].

current. By switching over from gyrotrons with current drive to gyrotrons without current drive at the right moment, the equilibrium current is reached within 5 s rather than in more than 20 s (see fig. 13). We conclude that the optimisation of W7-X for low bootstrap

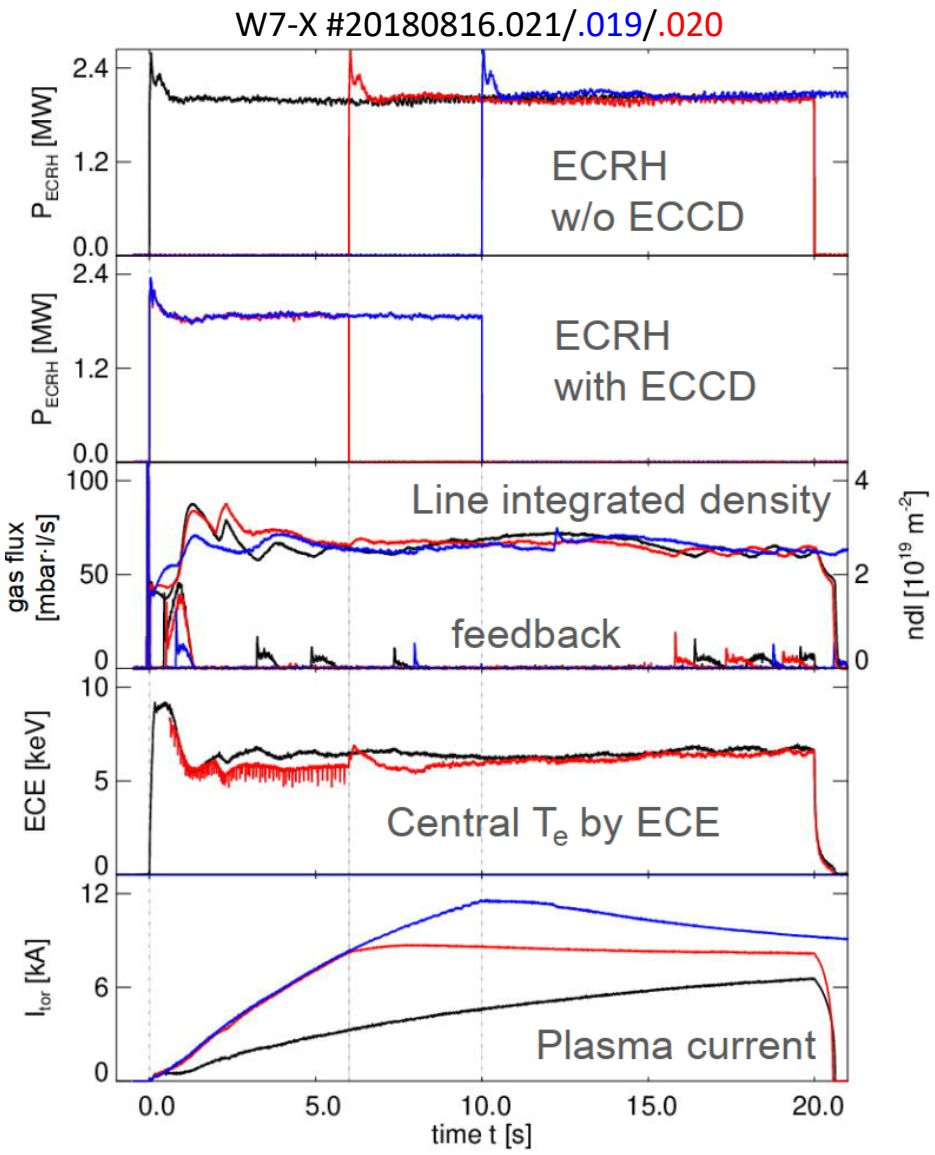

Figure 13: Comparison of a discharge without ECCD (black) with two discharges with ECCD in the same direction as the bootstrap current, for 10 s (blue), and for 5 s (red). ECRH power was the same in all three discharges, and it was kept constant within the discharges with current drive by switching over from gyrotrons with oblique launching angles to others with perpendicular launching (see top two panels). The current drive accelerates the evolution of the total current (see bottom panel). In the case shown in blue, the total curent increased to a value above the bootstrap current and started to decrease again once the current drive was switched off. In the case shown in red, the current drive was switched off in the "right" moment, such that the total current remained constant for the rest of the discharge. Figure adapted from [56].

currents was successful and that the remaining currents can be controlled, e. g. by ECCD.

4.3 Reduced neoclassical transport for thermal particles

One of the goals of the W7-X optimisation was the reduction of neoclassical transport by thermal particles relative to a "classical" stellarator. To verify whether this was successful, we investigate a particular type of discharge with pellet injection, represented by the time traces shown in fig. 14. The discharge starts at moderate heating power and low density. ECRH heats the electrons, therefore T_e is high, but T_i is low. The diamagnetic energy is small. In the time window highlighted in grey, a number of hydrogen pellets are injected. The density strongly rises. The density profile becomes peaked (not shown), and the electrons are cooled. At the end of the pellet injection phase, the heating power is increased by a factor of ~ 1.5. Electron and ion temperatures now both start rising, whereas the density decreases but stays peaked in the centre. The diamagnetic energy reaches a maximum of $\sim 1\,\mathrm{MJ}$ for $\sim 200\,\mathrm{ms}$, which is one energy confinement time. In this time interval, highlighted in light brown, the triple product is $n_\mathrm{i} T_\mathrm{i} \tau_\mathrm{E} \approx 5 \times 10^{19}\,\mathrm{keV\,s\,m^{-3}}$, which is very close to the record value for stellarators, the central β value is $\sim 4\,\%$, and $\langle\beta\rangle \approx 1\,\%$.

For this time interval, we use the measured density and temperature profiles for a calculation of the neoclassical energy transport in the electron and ions channels, as described in detail in [57]. We then normalise the calculated energy transport through each flux surface with the total heating power. Since neoclassical transport is the minimum conceivable transport, this ratio should always be < 1. Otherwise, the available heating power could not feed the calculated energy transport. The example discharge was performed in magnetic "standard" configuration, which has a particularly low value of the effective helical ripple ε_eff (see fig. 15). Indeed, the calculated neoclassical transport accounts for only about 1/3 of the energy losses at its maximum (see fig. 16). We can now for comparison calculate the neoclassical transport, assuming identical density and temperature profiles but different magnetic configurations with higher values of ε_eff. The results are also shown in fig. 16 for the W7-X "high-mirror" configuration and for two LHD configurations, the latter representing stellarator/heliotron configurations which are not particularly optimised for low neoclassical transport. Whereas the neoclassical transport in the W7-X "high-mirror" configuration would still be compatible with the observed profiles, they could not be achieved with such a low heating power in the two LHD configurations chosen for comparison.

We conclude that in a non-optimised stellarator, a significantly higher heating power than the applied 4.5 MW would be required to achieve the observed core temperatures and triple product.

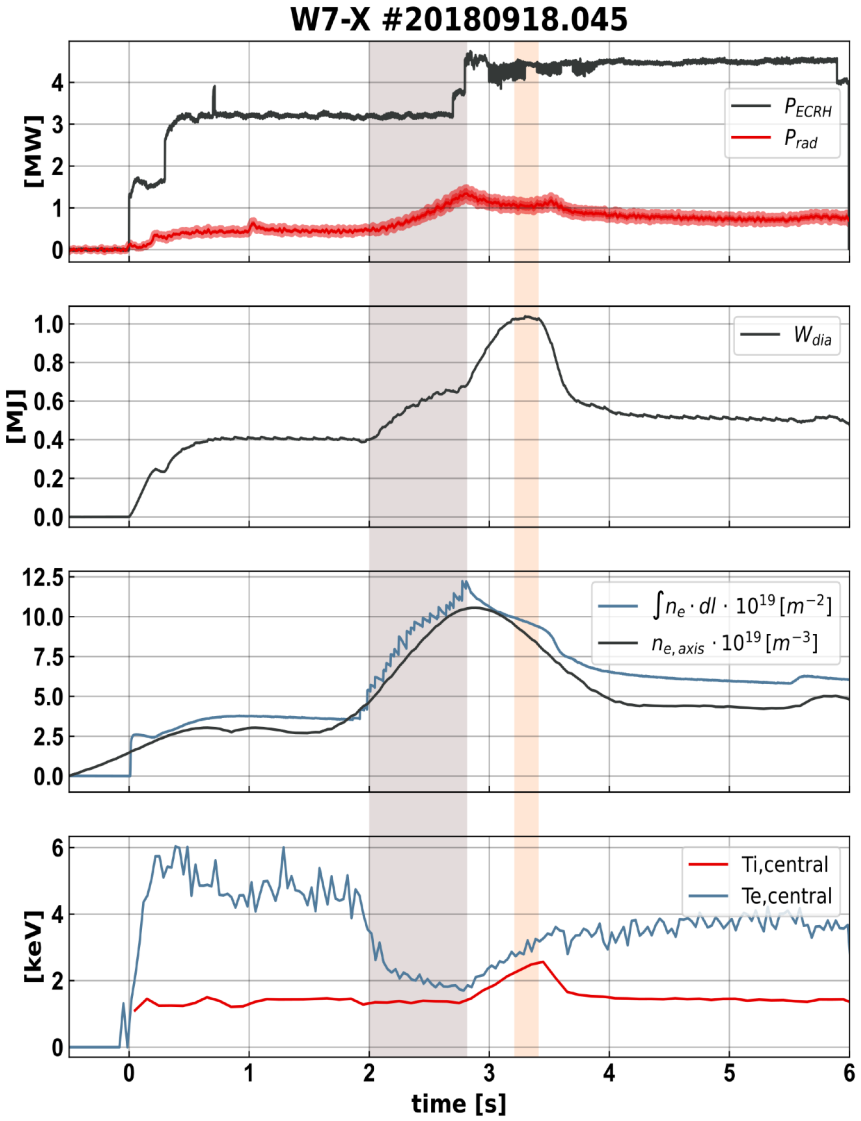

Figure 14: Discharge with hydrogen pellet injection during the time interval highlighted in grey and subsequent increase of the heating power. In consequence, the ion temperature rises together with the electron temperature, and an energy confinement time of $\sim 200\,ms$ and a diamagnetic energy of more than $1\,MJ$ is achieved within the interval highlighted in light brown.

4.4 Anomalous transport

Although the optimisation of the neoclassical transport was necessary to achieve the results reported in the previous section, we note from fig. 16 that even in time intervals with the lowest observed radial heat transport, the neoclassical contribution accounts for less than half of this observed transport, even at its radial maximum. Obviously, a large frac-

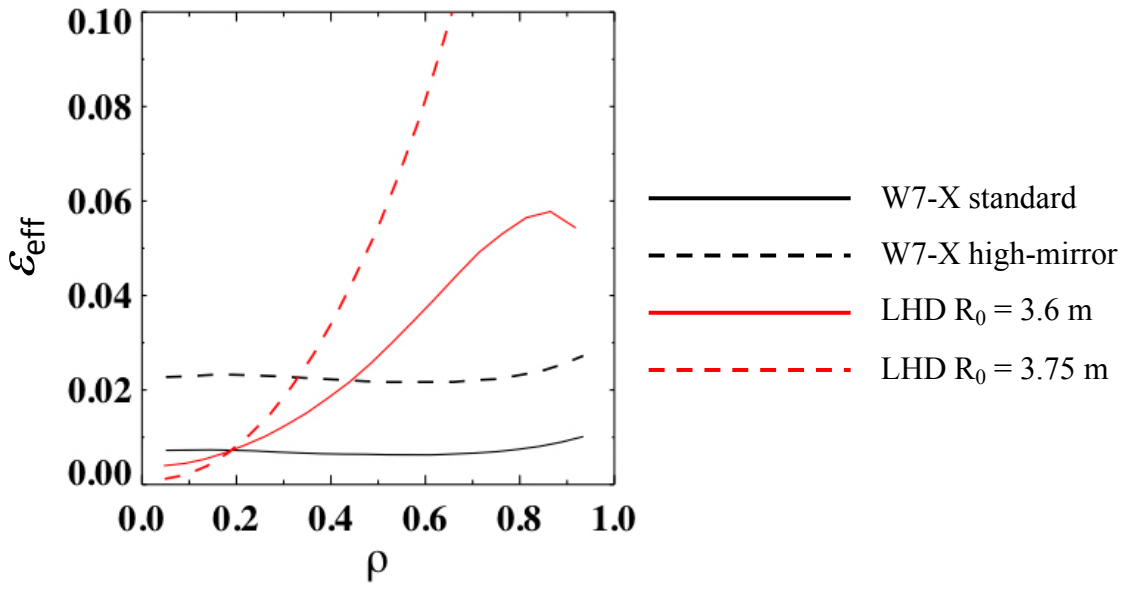

Figure 15: Effective helical ripple as a function of the normalised minor radius ρ for the W7-X "standard" and "high-mirror" magnetic configurations and for two LHD configurations [57]. ε_{eff} is a measure characterising the fraction of trapped particles in a magnetic configuration (see, e. g., [8, 9, 10]). A low value of ε_{eff} will reduce neoclassical transport for low collisionalities.

tion is "anomalous", i. e., presumably due to plasma turbulence. It is therefore interesting to compare fluctuation measurements between time intervals of good confinement like the one highlighted in light brown in fig. 14 and the periods before and after such intervals, and to consider what differences plasma turbulence theory would predict between these intervals.

Indeed, observations with the Phase Contrast Imaging (PCI) diagnostic [58] in discharges with pellet injection show a reduction of the fluctuation level during the intervals of good confinement [59] (see fig. 17 for an example from a discharge similar to that shown in fig. 14).

An investigation of the turbulence mechanisms on the ion gyroradius scale, which are believed to contribute most to turbulent transport in fusion devices, reveal an interesting property of magnetic configurations like the W7-X "standard" configuration, which have a maximum of the second adiabatic invariant J on the plasma axis: Between the conditions favouring the Ion Temperature Gradient (ITG) turbulence mechanism (high T_i gradients) and those favouring the Trapped Electron Mode (TEM) turbulence mechanism (high density gradients) there exists a region with reduced linear growth rates [60]. Such a stability valley [61] at similar radial scale lengths of density and ion temperature gradient does not exist in magnetic configurations without the "maximum-J" property, which includes tokamaks. The key to achieve improved confinement would then be the steepen-

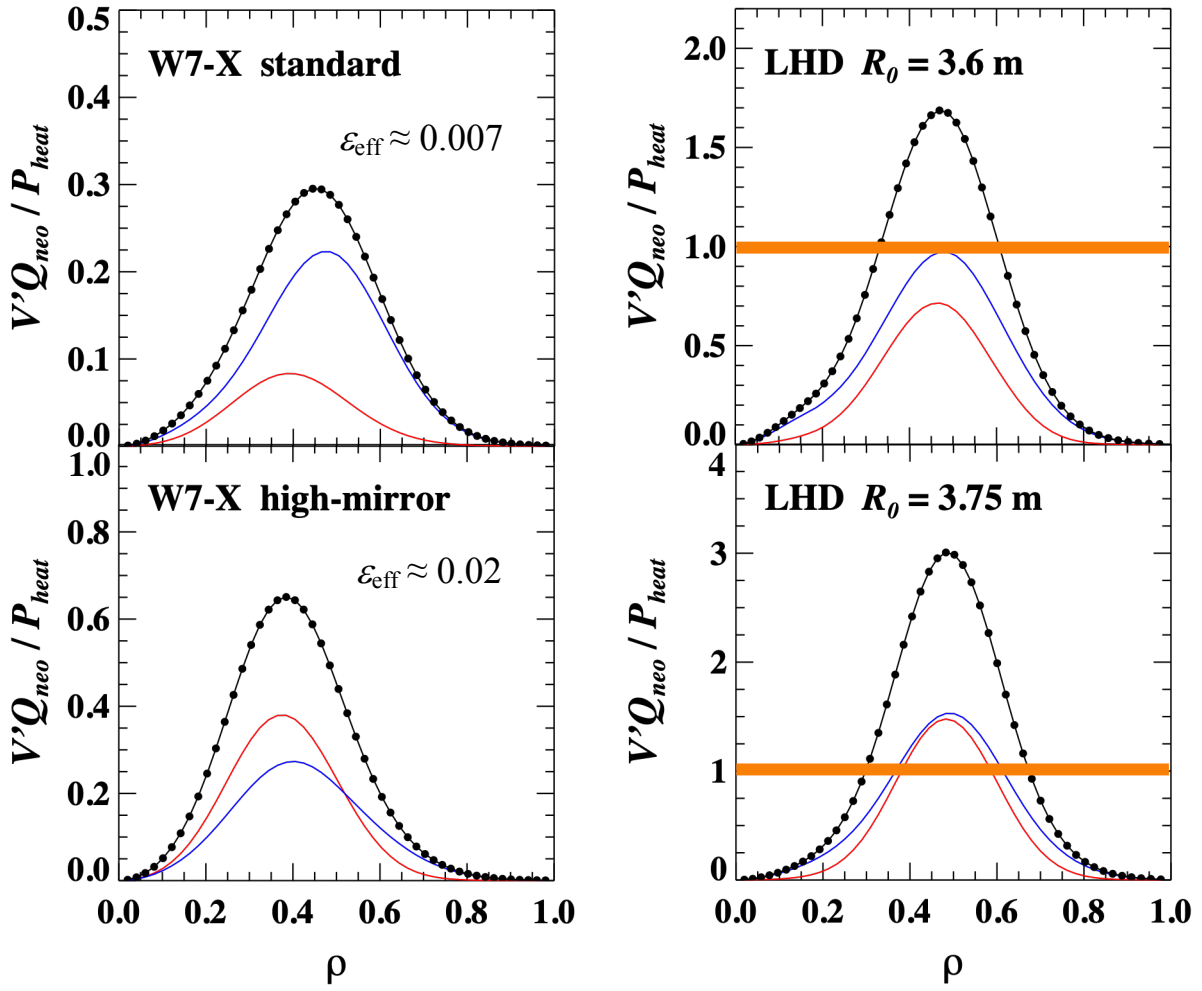

Figure 16: Neoclassical energy transport by electrons (red), ions (blue) and total (black), normalised by the heating power, calculated for measured density and temperature profiles during the interval highlighted in light brown in fig. 14 for four different magnetic configurations. The neoclassical transport is represented by the energy transport through the flux surface at the normalised minor radius ρ. The $\varepsilon_{\rm eff}$ profiles for the four magnetic configurations are shown in fig. 15. The results for the LHD confgurations are included as examples for configurations which did not undergo neoclassical optimisation. The transport values exceeding 1 indicate that in such magnetic configurations the observed density and temperature profiles would require a higher heating power. Figure adapted from [57]. A more detailed description, including a sensitivity analysis of the neoclassical results to uncertainties in the density and temperature measurements, can be found in that reference.

ing of the density gradient, here due to pellet injection, which permits also a steeper $T_{\rm i}$ gradient without leaving the stability valley. A reduced turbulent ion heat transport for

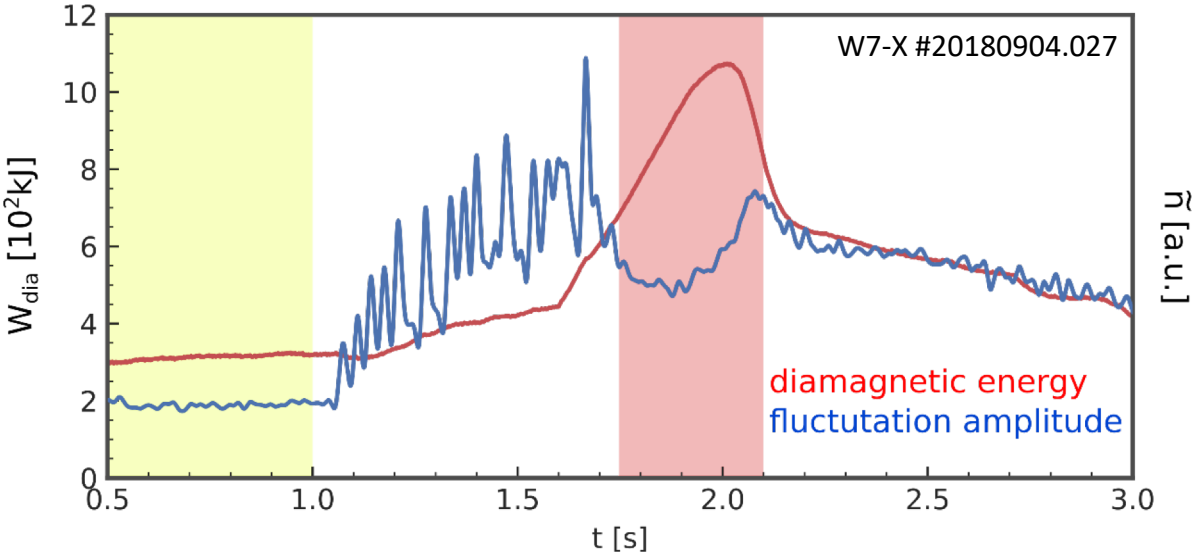

Figure 17: Amplitude of density fluctuations, measured by the phase contrast imaging diagnostic [58], during a discharge with pellet injection similar to that shown in fig. 14. Due to the pellet injection between 1.0 s and 1.7 s, strong density fluctuations are observed, which need not necessarily be related to turbulence. After that, the fluctuation amplitude exhibits a minimum during the strong increase of the diamagnetic energy and starts to increase again, while the diamagnetic energy is rolling over. It should be noted that, although the amplitude of fluctuations is not a direct measure of turbulent transport, a reduction of this amplitude for density fluctuations in spite of a simultaneous steepening of the density gradient (see text in section 4.3, not shown) is a strong indication of reduced turbulence.

the conditions established under pellet injection is as well found in nonlinear gyrokinetic simulations [62]. A steepening of the density gradient can also be achieved by NBI and probably by other means of profile control.

Since turbulence often increases energy, bulk particle and impurity density transport in a similar way, the turbulent transport can also be assessed by the comparison of impurity transport after laser ablation between discharges with flat density profile and with steeper density gradient: The impurity transport is indeed found to be significantly smaller for steeper density gradients [59].

These observations may open a path to reduced turbulent transport. Further investigations of this topic will certainly form an important part of the next experimental campaign on W7-X.

4.5 Steps toward stationary discharges

The goal of demonstrating stationary high-power discharges in W7-X implies stationarity on the longest plasma physics time scale, which is the L/R time for the establishment of a toroidal plasma current (bootstrap current), of the order of several 10 s. It also implies that processes influencing plasma operation are stationary, including outgassing of wall components, and, on a technical level, that the temperatures of all components become stationary. This may take a few seconds for the highest loaded target elements, and a few minutes for the low loaded plasma facing components. For components behind the first wall which only receive small heat fluxes through gaps in the first wall or from thermal radiation or microwave stray radiation and which are therefore not actively cooled, this may still take longer.

A large step toward less impurity production and higher density in longer plasma discharges was the first boronisation in the beginning of OP1.2b. This strongly reduced impurities, in particular oxygen [63, 64] (see fig. 18). The effect lasted not only for a few

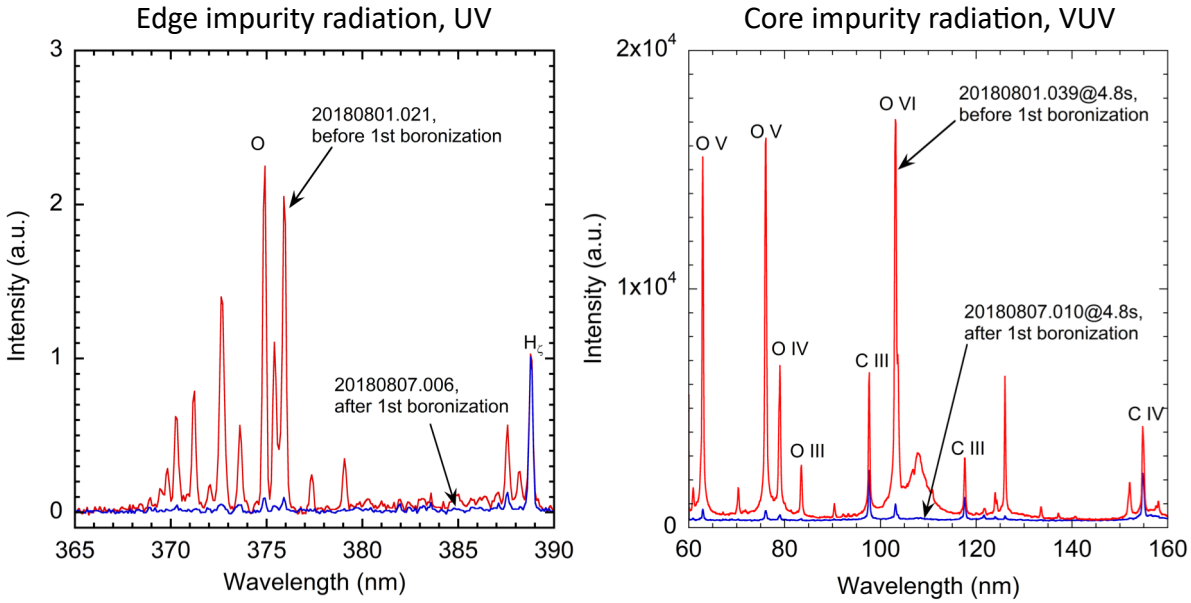

Figure 18: Impurity line radiation in comparable discharges before (red) and after (blue) the first boronization of W7-X, measured in the ultraviolet with the divertor spectrometer (left) [63], and in the VUV with the HEXOS spectrometer (right) [64]. Notably the oxygen and carbon content is significantly reduced after boronization.

discharges after boronisation, but actually for several weeks. This is also reflected in the Z_{eff} values and the achieved plasma densities before and after boronisation.

To understand the effect on plasma density, it is important to note that no disruptive density limit has been observed in stellarators. Instead, the plasma density is limited by a radiation collapse, if the heating power is no longer sufficient to balance the radiation

losses [65, 66]. The empirical formula

$$\bar{n}_\mathrm{c} = c\,\frac{{P_\mathrm{heat}}^{0.6}}{{f_\mathrm{imp}}^{0.4}} \tag{1}$$

has been derived from experimental data [66], where $\bar{n}_\mathrm{c}$ is the limit of the average plasma density and

$$f_\mathrm{imp} = n_\mathrm{imp}/n_\mathrm{e}$$

is the impurity fraction. For a limited heating power, high-density operation therefore requires the control of the impurity content in the discharge. In consequence, significantly higher densities could be reached with the same heating power after boronisation (see fig. 19).

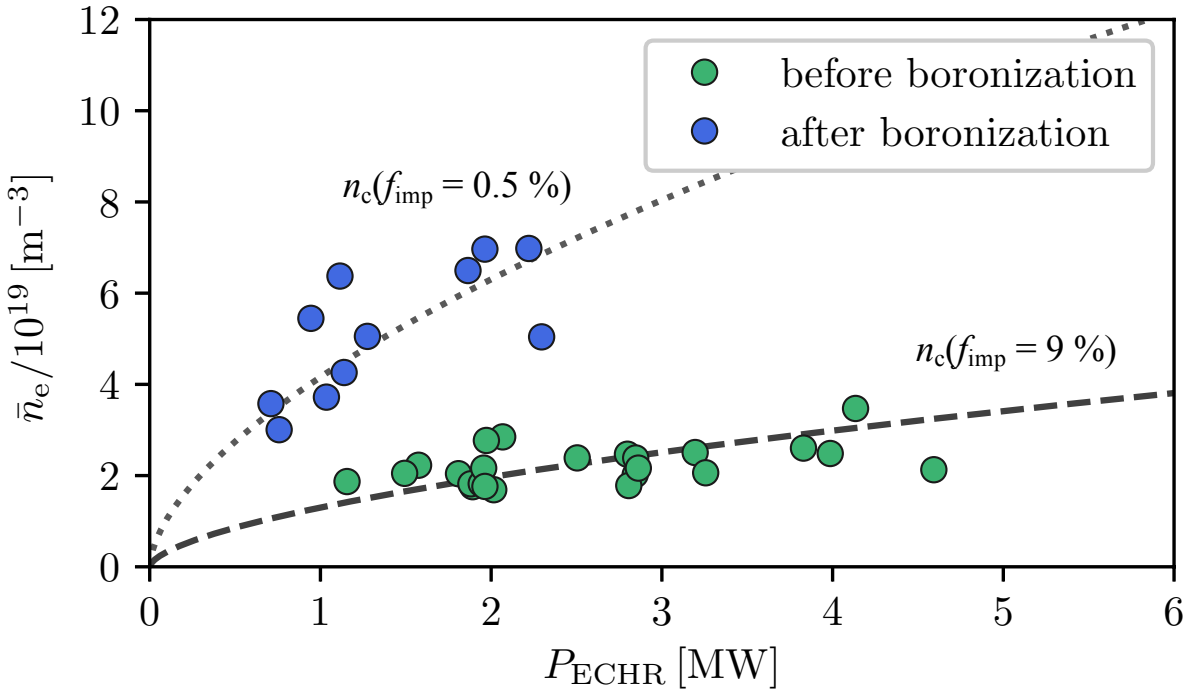

Figure 19: Maximum average density in magnetic "standard" configuration as a function of heating power before and after the first boronization. The impurity fraction used in eq. (1) to obtain the two curves is indicated. Due to the reduced impurity content after boronization, W7-X could be operated at significantly higher plasma density for a given heating power.

The higher plasma density goes along with higher neutral density at the targets and behind the target plates. This results in better pumping efficiency and better density control [67].

The high density also facilitates detachment of the plasma from the target plates. This is a favourable operating condition, where a cloud of high neutral density forms between

the X-points and the target plates and strongly reduces the plasma particle and heat flux onto the targets. An example is given at the end of this section in fig. 21.

At the end of the last experimental campaign OP1.2b the power limit of 80 MJ was suspended and the length of the discharge was stepwise increased. In fig. 20, the result

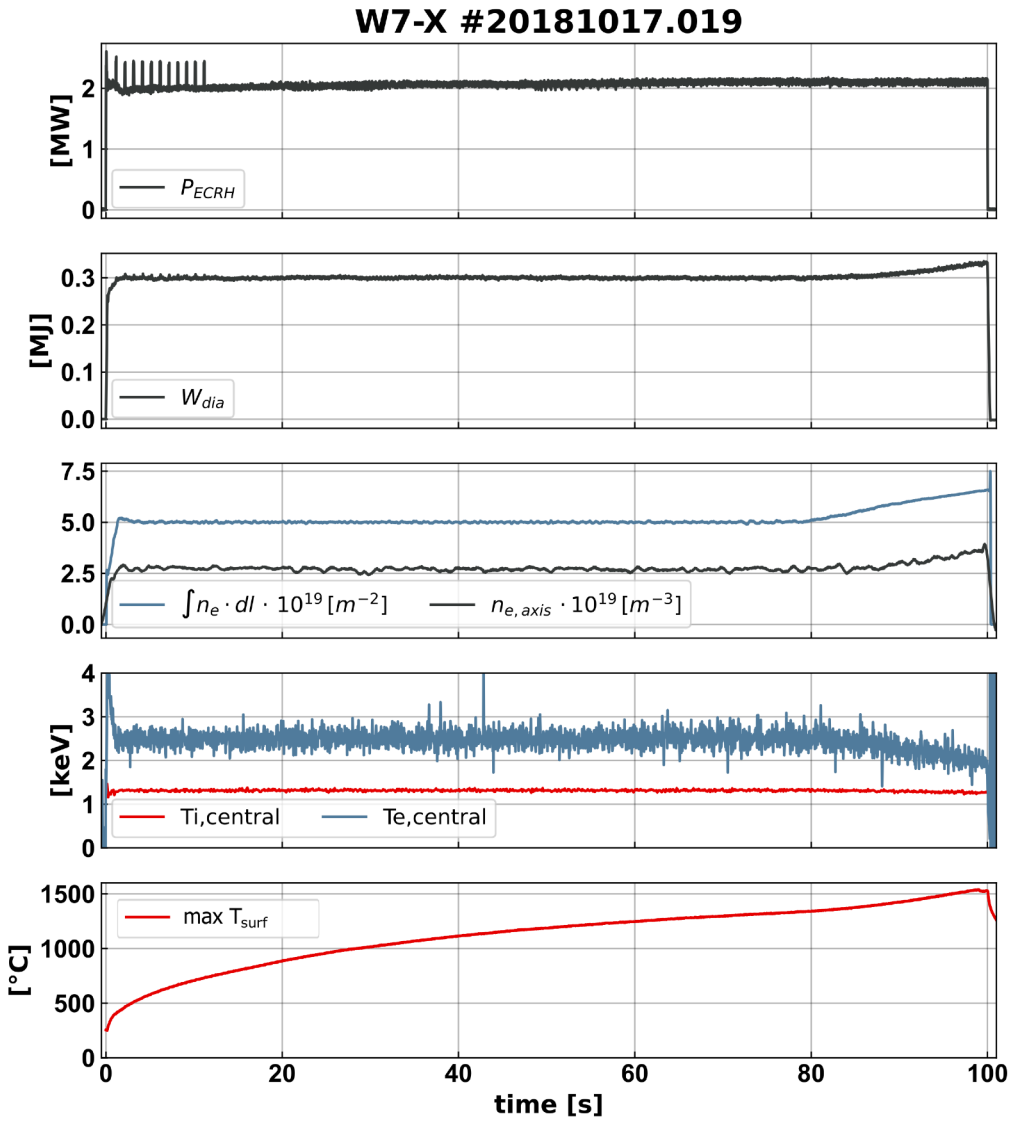

Figure 20: Discharge with 2 MW heating power for 100 s. Plasma density, electron and ion temperatures and diamagnetic energy stay stationary for 80 s, however, the temperature of the uncooled targets is constantly increasing. After 80 s, outgassing becomes too strong, such that the density starts rising although the gas valves are closed by feedback control.

at a low heating power of 2 MW is shown [68]. A total of 200 MJ was injected in a 100 s discharge. For 80 s, plasma density, electron and ion temperatures and plasma energy can be kept constant. The temperature of the uncooled targets is constantly rising. The gas

flux required to keep the density is constantly reducing (not shown), until the discharge is fed exclusively by outgassing, and the density starts rising. However, in the series of stepwise extended discharges, this loss of density control still shifted to ever later times, indicating that conditioning of the critical gas reservoirs was still ongoing.

In our second example for long stationary discharges, 5 MW of heating power were applied, and the plasma density was kept at about twice the value of our first example (see fig. 21). After ~ 2.5 s, the plasma detaches from the targets: The radiated power

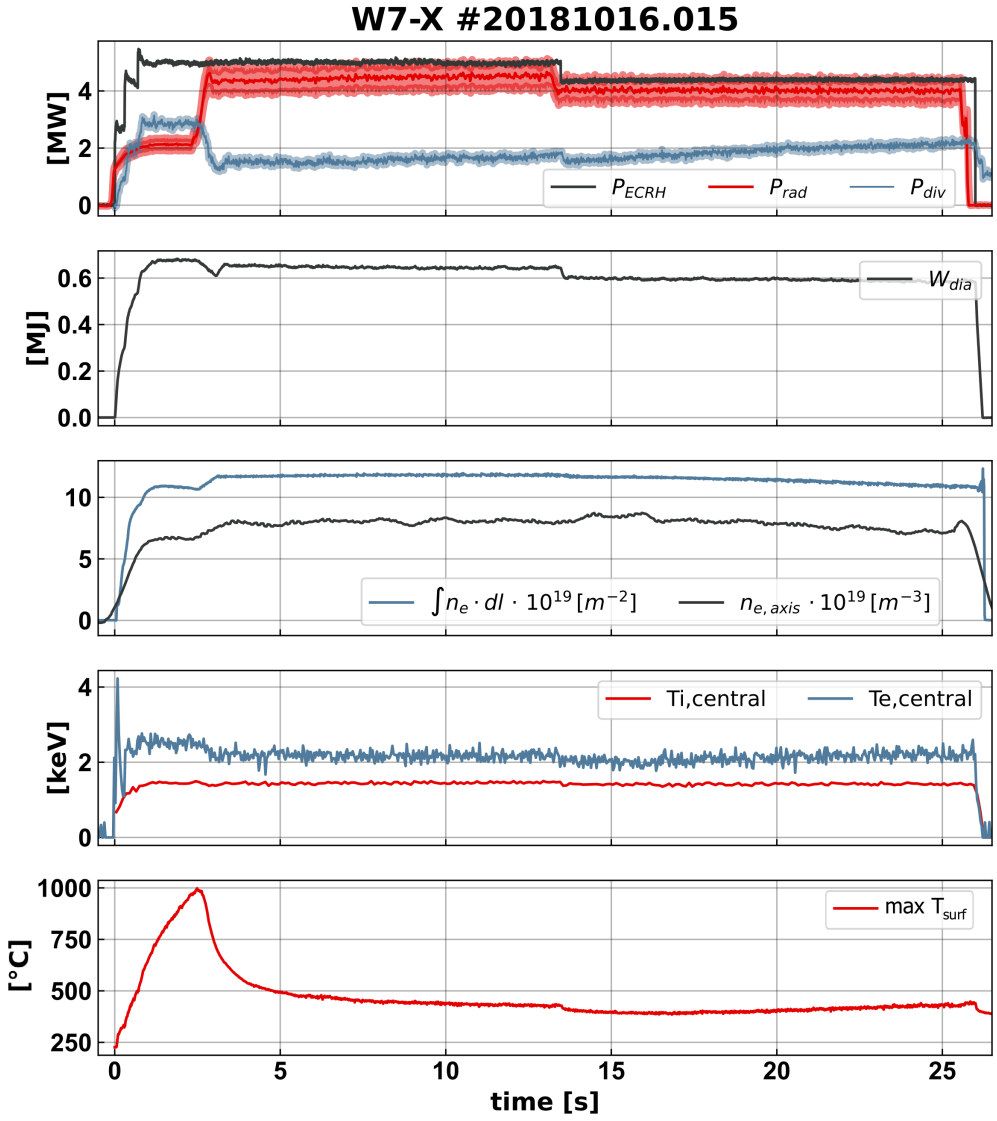

Figure 21: Discharge with 5 MW heating power and stationary conditions under stable detachment for 25 s. Divertor detachment starts at ~ 2.5 s: The radiated power reaches almost the heating power, and the maximum divertor temperature drops to below 500° C, whereas central electron and ion temperatures remain unaffected.

increases almost to the heating power level, whereas the power to the targets drops. Consequently, the divertor temperature drops, and its maximum stays below 500° C for the entire rest of the discharge. Z_{eff} stays constant at a low value, the neutral pressure behind the divertor is high, but the plasma particle flux to the targets themselves remains low [67] (not shown here). We conclude that for this time interval of almost 25 s W7-X could be operated in a stable, thermally fully detached island divertor regime.

5 Prospect of next experimental campaigns

5.1 Device upgrades

The most prominent upgrade for the coming OP2 is the transition to the water-cooled HHF divertor and full water cooling of all plasma facing components. This does not only imply the exchange of the divertor units inside the plasma vessel but also the construction of an extensive system of pipes in the torus hall for supplying and distributing the cooling water. To give an impression of the complexity of this pipework, a CAD view of part of it is shown in fig. 22. Since the real heat loads in different locations of the targets and baffles cannot be modelled accurately in advance, a real-time monitoring system of those components receiving high heat load will be implemented, based on infrared cameras [69].

The 10 new cryopumps behind the horizontal targets [37] will be cooled by liquid He and will add a pumping speed of 75 000 l/s (in deuterium) to about 30 000 l/s provided by the 30 existing turbo molecular pumps.

The steady-state pellet injector [38] can generate up to 10 pellets per second of 3 mm diametre and 3 mm length.

For ECRH, one additional newly developed gyrotron with 1.5 MW nominal power will become available for OP2 [70, 71]. Subsequently, it is planned to further increase ECRH power by another 1.5 MW gyrotron and to successively replace the existing 1 MW gyrotrons. The addition of two ion sources will double the available NBI power to ~ 7 MW. Each source can work in pulses of 10–30 s. An interlock system will assure the fast shutdown of the beams if required [72]. The new ICRH system will be initially available with 1.5 MW at 37.5 MHz for hydrogen heating in pulses of 10 s every 300 s [20, 73]. A later upgrade is planned to 4 MW and for further heating scenarios (e. g., ^{3}He minority heating at 27 MHz) [21].

A number of diagnostics will also be upgraded, exchanged or newly added. No comprehensive list will be given here, but as examples we mention the following:

- The number of observed scattering volumes along the Thomson laser beam will be increased to improve the spatial resolution in the plasma edge. A second laser with different wavelength will be added, which allows to extend the range of observable

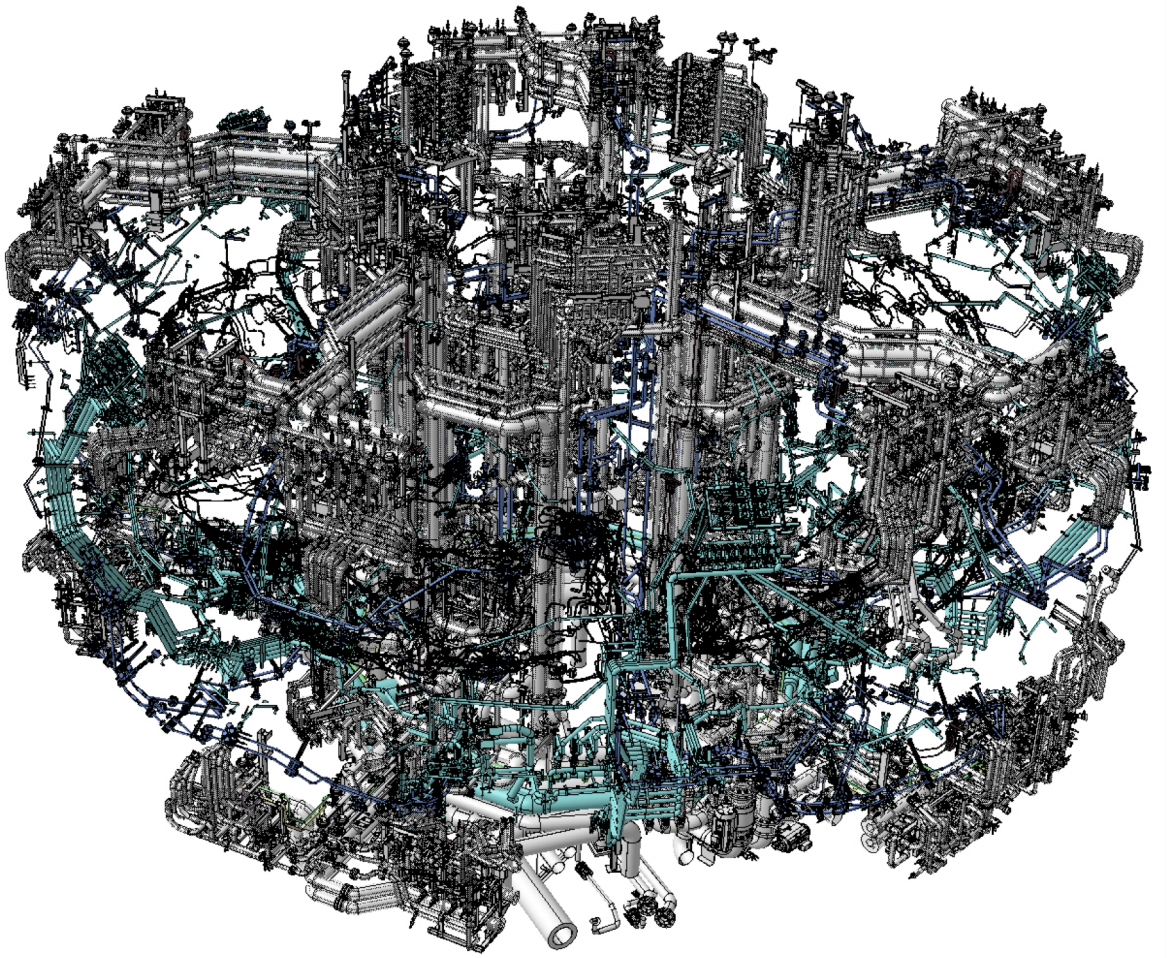

Figure 22: CAD view of cooling pipes. Only the pipe sections close to but outside the W7-X vessel are shown. The view contains all water pipes, comprising those for cooling the targets, baffles and remaining first wall, diagnostics, ports and plasma vessel as well as the island control and trim coils, plus the stray radiation shield of the cryopumps and the system for filling and draining the pipework. The total length of pipes is $\sim 2.5\,km$.

electron temperatures toward higher values without the need to change the optical filters [74].

- The Langmuir probes integrated into the TDU targets [75] will be replaced by pop-up probes to support long-pulse operation.
- A divertor manipulator will be added to expose material samples and to bring magnetic and electrical probes of different types into the edge plasma close to the targets, carry temperature sensors and also to feed gas into the plasma edge [76, 77]. The divertor manipulator will provide a chance to test standard, but also

innovative materials, material compositions and diagnostic concepts under high heat load conditions (up to $10\,\mathrm{MW/m^2}$), allowing a detailed investigation of the near-divertor plasma region by means of a dedicated observation system foreseen for the direct supervision of the exposed probes.

- A gas puff imaging (GPI) diagnostic will be built for two-dimensional observation of fluctuations in the edge islands (for the general concept of GPI, see, e. g., [78]).

- A Faraday cup style detector for fast particles [79] will be tested, initially on a manipulator. If successful, detectors of this type, with a high spatial resolution and a very flat design, could be distributed onto wall protection tiles in various locations of interest within the plasma vessel.

5.2 Focus of OP2 programme

From the overall goals of the W7-X project and from the results of the previous operational phases, several focal points of the programme for the next operational campaign become evident:

Since not all locations on the target surface support the same power density of up to $10\,\mathrm{MW/m^2}$, it will be important to have full control of the strike line position, in particular during the phase of toroidal current evolution. One way to control the edge rotational transform is ECCD. As demonstrated in section 4.2, it can be either used to counteract the evolving toroidal current, or to speed up the transition to its stationary value. Other schemes would be to use the complicated dependence of the bootstrap current on density and pressure to keep it constant by a coordinated increase of density and heating power [80], or the adjustment of the planar coil currents. Any of these methods, or a combination of them, must be developed to routine use to achieve strike line control, in particular during the transient start-up phase toward stationary toroidal plasma current.

Even with strike line control, it appears preferable to operate the divertor under detached conditions. It is therefore planned to develop stable detachment in different magnetic configurations to be able to operate the targets under reduced load.

With these ingredients and with full water cooling of all plasma facing components operational, the heating energy limit per discharge will be lifted stepwise. In the end, we want to demonstrate high-performance discharges with stationary conditions on all signals, which requires full density and impurity control.

As discussed in section 4.3, the improved neoclassical transport of thermal particles has been demonstrated. It has been found, however, that now the anomalous transport dominates. In a joint effort of theory and experiment, we want to understand better this turbulent transport and explore regimes of improved confinement. One first path toward this goal has opened during OP1.2b in pellet or NBI fuelled discharges, and a key seems

to be the right combination of density and temperature gradients in the core plasma. An experimental task will therfore be the development of density and temperature profile control.

With NBI and ICRH available for the generation of fast particles, investigation of their confinement in different magnetic configurations will start, including tests of suitable diagnostic methods. Since improved confinement of fast particles in W7-X requires volume-averaged β values of at least 2–3 %, the corresponding optimisation of W7-X can probably not be demonstrated before the available heating power is significantly enhanced (or the device is operated at reduced magnetic field).

5.3 Longer-term planning

An upgrading of the different heating systems has already been announced in section 5.1, but this will be a stepwise process, which will take several years. It was already foreseen in the earliest project schedules and is required to achieve a sufficiently high plasma pressure for the investigation of the expected MHD stability and also for the demonstration of improved fast particle confinement, which depends on the existence of a magnetic well due to the diamagnetic effect of the plasma.

Deuterium operation is planned to explore the existence of an isotope effect in this device, and to benefit from the higher NBI heating power in deuterium.

A further long-term project is the test of tungsten as a first wall material. A few tungsten tiles were already installed during OP1.2, without observing any traces of tungsten spectroscopically in the plasma. In OP2, an additional number of graphite wall protection tiles will be replaced by tungsten tiles. At the end of the process, targets with a tungsten surface should be installed. Although encouraging results with an all-tungsten first wall exist from tokamaks, we cannot entirely rely on this experience, since stellarators have impurity transport properties different from tokamaks. As carbon is not an acceptable wall material for a fusion reactor, it is an important task for W-X to explore the suitability of reactor-relevant wall materials in a stellarator.

6 Progress toward a fusion reactor

Comparing the performance of W7-X with that of other present-day and next-step devices in a Kikuchi diagram [81, fig. 3.16 and appendix of ch. 3] (see fig. 23, [36]), we started rather modestly in the limiter campaign, OP1.1. As soon as divertor operation started (OP1.2), we attained record triple products comparable with those of LHD for brief intervals of 200 ms. At the end of OP1.2, the two long discharges presented in section 4.5 are already close to the boundary line drawn in the Kikuchi diagram by large tokamaks. With water-cooled targets in OP2, we envisage discharge intervals with the same duration as planned for ITER.

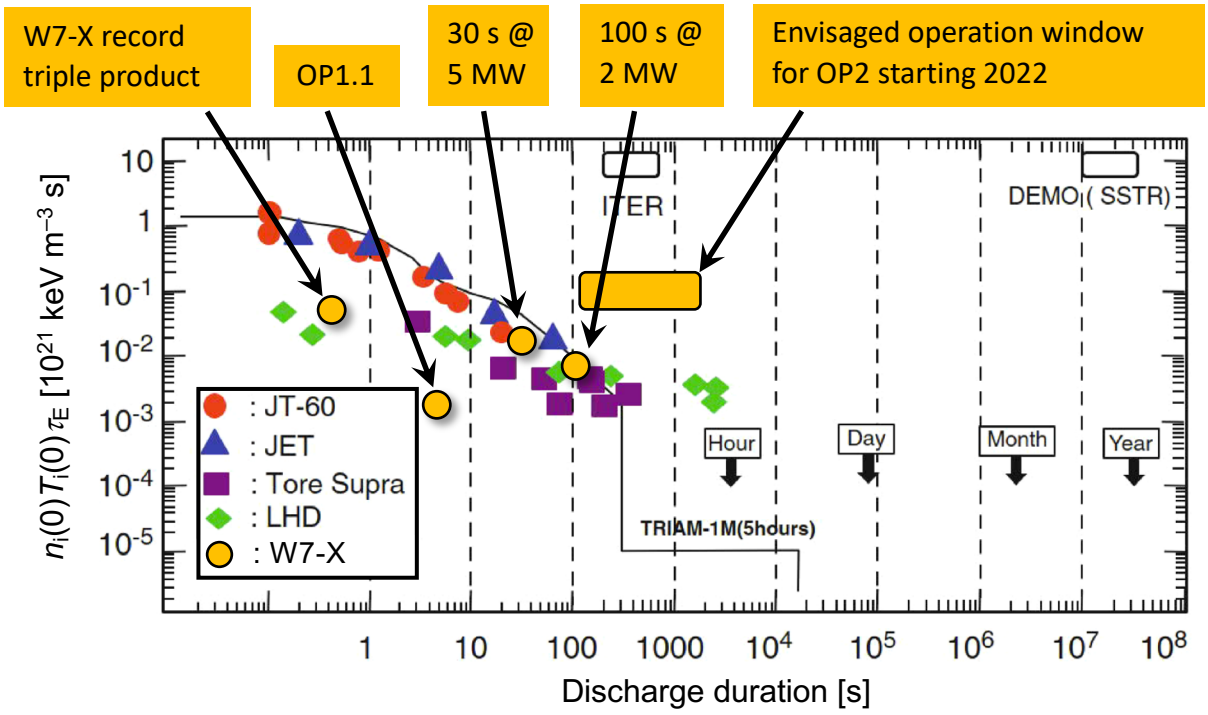

Figure 23: Kikuchi diagram [81] with operation points of W7-X in the past experimental campaigns and the envisaged window for the next operational phase [36, 35] in comparison with other large existing and planned fusion experiments. This figure is an adapted version of fig. 3.16, published in and reproduced with permission from Springer: M. Kikuchi and M. Azumi, Frontiers in Fusion Research II, *Springer, Cham 2015 (https://doi.org/10.1007/978-3-319-18905-5). Copyright 2015.*

Simultaneously, studies for technical components are ongoing, which for a stellarator reactor might differ significantly from a tokamak reactor (see [82] for an example). Furthermore, system-level studies are being performed to investigate the impact of size and configuration of a stellarator reactor on performance and to assess such a helical axis advanced stellarator (HELIAS) as a next-step device (see [83, 84] for examples).

To bridge the gap to a fusion reactor, W7-X can serve several purposes, as will be detailed in the following two sections.

6.1 Testbed for steady-state operation

As becomes evident from the positioning of the W7-X OP2 in the Kikuchi diagram, several individual components and their interplay can be tested in intervals as planned for ITER operation. This is true for the cw gyrotrons developed for W7-X ECRH, which repeatedly set new benchmarks, and for the steady-state pellet injector developed for ITER [38]. All in-vessel components, including various diagnostics, have been designed for an increased

level of microwave stray radiation [85, 86, 87, 88]. A number of diagnostics adaptations were developed, which are also relevant for ITER, e. g., neutral gas pressure gauges using heated crystals as electron emitters [89] rather than wire filaments, which showed to be thermo-mechanically unstable in long discharges.

For machine control, the concept of subdividing a discharge program into segments was developed [90]. For these segments, execution may depend on certain conditions, which may be derived from quantities measured by sensors, e. g. plasma diagnostics [91]. Measurement data are continuously recorded and streamed to the central storage system [92, 93]. They are provided with time stamps, allowing, in principle, a synchronisation with an accuracy of order 10 ns [94].

For all these systems, W7-X operation provides experience under realistic long-pulse operating conditions.

6.2 Validation and improvement of theoretical foundations

While the topics listed in the previous section are important contributions to the operation of ITER and a next-step fusion experiment, the major goal of the W7-X project is to provide experimental results which allow the testing and further development of the theoretical basis for stellarator optimisation, which will then serve as a foundation for the design of a future stellarator reactor.

The achievement of reduced collisional transport (section 4.3) and low bootstrap current (section 4.2) confirm the optimisation based on neoclassical theory. In future experimental campaigns, the optimisation for low transport of fast particles and MHD stability at high β values will have to be validated. At the same time, the future optimisation of magnetic configurations and operating scenarios will include turbulence and edge and divertor physics. W7-X, as an existing device, will have the task of contributing the experimental basis for the underlying models.

7 Conclusions

In the first three W7-X operational phases, the achievement of several project goals could already be demonstrated: The magnet system of non-planar superconducting coils could be built with very good accuracy, and reduced neoclassical transport of thermal particles and low bootstrap current were found, confirming the optimisation based on neoclassical transport theory.

The (still uncooled) island divertor was operated successfully in different magnetic configurations. After boronisation, low impurity content and high plasma densities were achieved. At low plasma density and low heating power, discharges were conducted for up to 100 s under stationary conditions (except for the divertor temperature and related outgassing). At higher plasma density and heating power, stable divertor detachment

was demonstrated for up to 26 s (at constant temperature of the uncooled divertor!). No impurity accumulation was observed. The installation of the water-cooled High Heat Flux divertor and of water cooling for all in-vessel components will allow us to extend stationary operation to still longer intervals, in agreement with the project goals.

While energy confinement times of 200 ms at high plasma density, electron and ion temperatures of 2–3 keV and a triple product $n_\mathrm{i} T_\mathrm{i} \tau_\mathrm{E} \approx 5 \times 10^{19}\,\mathrm{keV\,s\,m^{-3}}$ were achieved for short intervals under special conditions, the confinement was found to be inferior to the level expected from neoclassical theory during most of the time. Turbulent transport is the suspected candidate for this "anomalous" transport. Comparison of the level of density fluctuations during "good" and "poor" confinement intervals corroborates this view. Although the optimisation of the neoclassical transport is imperative for a stellarator reactor, it is not sufficient for obtaining "good" confinement, as is well known from the tokamak world. However, the observation of improved confinement during intervals with peaked density profiles is in agreement with newer turbulence modelling, which predicts reduced instability against ITG/TEM driven turbulence for a certain class of magnetic configurations, if ion temperature and density gradient scale lengths are close to each other. The experimental and theoretical exploration of improved confinement regimes will certainly be an important focus during the next operational phase of W7-X. This will require methods to control the radial density and temperature *profiles* in W7-X.

In a reactor, a large fraction of the heat must be radiated rather than deposited in narrow strike lines on the targets. We will therefore have to develop scenarios for stable detachment under different operating conditions. In addition, strike line position control must be further developed to protect sensitive areas of the target surface during the non-stationary phase at plasma startup.

With increased NBI power and ICRH becoming available for the next operational phase, the investigation of fast particle confinement will be intensified. Good neoclassical confinement of fast particles is only predicted for certain magnetic configurations and only at sufficiently high β values. To achieve such a high plasma pressure requires a further increase of the heating power, which is also necessary to verify the MHD stability at high β.

A longer-term plan is the replacement of carbon first-wall components by tungsten, with the final goal of pure tungsten or tungsten-coated targets, to investigate whether the impurity transport properties allow the operation of an "all-tungsten" stellarator.

It is thus the task of the W7-X project to provide all necessary experimental information and the theoretical base to design a next-step device as stellarator.

Acknowledgements

We thank F. Herold, M. Krause, R. Laube and the W7-X Design Engineering department for contributing several CAD views and T. Andreeva and J. Kißlinger for providing the

graphics highlighting the edge islands in perturbed and unperturbed magnetic field.

This work has been carried out within the framework of the EUROfusion Consortium and has received funding from the EURATOM research and training programme 2014–2018 and 2019–2020 under grant agreement no. 633 053. The views and opinions expressed herein do not necessarily reflect those of the European Commission.

References

[1] T. Klinger et al. Overview of first Wendelstein 7-X high-performance operation. *Nuclear Fusion*, **59**(11) 112004, November 2019.

[2] G. Grieger, W. Lotz, P. Merkel, J. Nührenberg, J. Sapper, E. Strumberger, H. Wobig, W7-X Team, R. Burhenn, V. Erckmann, U. Gasparino, L. Giannone, H. J. Hartfuß, R. Jaenicke, G. Kühner, H. Ringler, A. Weller, F. Wagner, and W7-AS Team. Physics optimization of stellarators. *Physics of Fluids B: Plasma Physics*, **4**(7) 2081–2091, July 1992.

[3] J. Nührenberg and R. Zille. Quasi-helically symmetric toroidal stellarators. *Physics Letters A*, **129**(2) 113–117, 9 May 1988.

[4] C. Beidler, G. Grieger, F. Herrnegger, E. Harmeyer, J. Kißlinger, W. Lotz, H. Maaßberg, P. Merkel, J. Nührenberg, F. Rau, J. Sapper, F. Sardei, R. Scardovelli, A. Schlüter, and H. Wobig. Physics and engineering design for Wendelstein VII-X. *Fusion Technology*, **17**(1) 148–168, January 1990.

[5] H.-S. Bosch et al. Technical challenges in the construction of the steady-state stellarator Wendelstein 7-X. *Nuclear Fusion*, **53**(12) 126001, December 2013.

[6] L. Wegener, J.-H. Feist, J. Sapper, F. Kerl, and F. Werner. Final design and construction of the Wendelstein 7-X coils. *Fusion Engineering and Design*, **58–59** 225–230, November 2001. Proceedings of the 21st Symposium on Fusion Technology, Madrid, Spain, 11–15 September 2000.

[7] M. Nagel, A. Braatz, A. Gömöry, S. Hughes, Ch. Heenemann, S. Mohr, M. Pietsch, K. Risse, D. Theuerkauf, A. Binni, M. Prebeck, and H. Posselt. Design and assembly progress of the thermal insulation of the Wendelstein 7-X cryostat. In *Proceedings of the 23rd International Cryogenic Engineering Conference and International Cryogenic Materials Conference 2010, ICEC23-ICMC 2010, Wroclaw, Poland*, pages 815–820, 2010.

[8] C. D. Beidler, K. Allmaier, M. Yu. Isaev, S. V. Kasilov, W. Kernbichler, G. O. Leitold, H. Maaßberg, D. R. Mikkelsen, S. Murakami, M. Schmidt, D. A. Spong, V. Tribal-

dos, and A. Wakasa. Benchmarking of the mono-energetic transport coefficients—results from the International Collaboration on Neoclassical Transport in stellarators (ICNTS). *Nuclear Fusion*, **51**(7) 076001, July 2011.

[9] Per Helander. Theory of plasma confinement in non-axisymmetric magnetic fields. *Rep. Prog. Phys.*, **77**(8) 087001, August 2014.

[10] A. Dinklage, C. D. Beidler, P. Helander, G. Fuchert, H. Maaßberg, K. Rahbarnia, T. Sunn Pedersen, Y. Turkin, R. C. Wolf, A. Alonso, T. Andreeva, B. Blackwell, S. Bozhenkov, B. Buttenschön, A. Czarnecka, F. Effenberg, Y. Feng, J. Geiger, M. Hirsch, U. Höfel, M. Jakubowski, T. Klinger, J. Knauer, G. Kocsis, A. Krämer-Flecken, M. Kubkowska, A. Langenberg, H. P. Laqua, N. Marushchenko, A. Mollén, U. Neuner, H. Niemann, E. Pasch, N. Pablant, L. Rudischhauser, H. M. Smith, O. Schmitz, T. Stange, T. Szepesi, G. Weir, T. Windisch, G. A. Wurden, D. Zhang, and W7-X Team. Magnetic configuration effects on the Wendelstein 7-X stellarator. *Nature Physics*, 2018.

[11] H. Renner, J. Boscary, V. Erckmann, H. Greuner, H. Grote, J. Sapper, E. Speth, F. Wesner, M. Wanner, and W7-X Team. The capabilities of steady state operation at the stellarator W7-X with emphasis on divertor design. *Nuclear Fusion*, **40**(6) 1083–1093, June 2000.

[12] Daniel Böckenhoff, Marko Blatzheim, and W7-X Team. Application of improved analysis of convective heat loads on plasma facing components to Wendelstein 7-X. *Nuclear Fusion*, **59**(8) 086031, August 2019.

[13] Hermann Renner, Devendra Sharma, Johann Kißlinger, Jean Boscary, Heinz Grote, and Ralf Schneider. Physical aspects and design of the Wendelstein 7-X divertor. *Fusion Sci. Tech.*, **46**(2) 318–326, September 2004. Special Issue: Fourteenth International Stellarator Workshop (Part 2), Greifswald, Germany, September 22–26, 2003.

[14] Frank Füllenbach, K. Risse, T. Rummel, P. van Eeten, A. Carls, O. Volzke, M. Haas, H.S. Bosch, and W7-X Team. Commissioning of the Wendelstein 7-X in vessel control coils. *IEEE Trans. Plasma Sci.*, **48**(7) 2635–2638, July 2020. Special Issue on Selected Papers from 27th Symposium on Fusion Engineering (SOFE), Princeton, NJ, 2017.

[15] Jiawu Zhu, Victor Bykov, Gunnar Ehrke, Boris Mendelevitch, Dirk Naujoks, Lutz Wegener, and Hans-Stephan Bosch. Multiphysics analysis of W7-X control coils. *Fusion Engineering and Design*, **146A** 1369 – 1372, September 2019. Proceedings of the 30th Symposium on Fusion Technology (SOFT-30), Giardini Naxos, Sicily, Italy, September 16–21, 2018.

[16] V. Erckmann, P. Brand, H. Braune, G. Dammertz, G. Gantenbein, W. Kasparek, H. P. Laqua, H. Maassberg, N. B. Marushchenko, G. Michel, M. Thumm, Y. Turkin, M. Weissgerber, A. Weller, W7-X ECRH Team at IPP Greifswald, W7-X ECRH Team at FZK Karlsruhe, and W7-X ECRH Team at IPF Stuttgart. Electron cyclotron heating for W7-X: Physics and technology. *Fusion Sci. Tech.*, **52**(2) 291–312, August 2007.

[17] Norbert Rust, Bernd Heinemann, Boris Mendelevitch, Alan Peacock, and Michael Smirnow. W7-X neutral-beam-injection: Selection of the NBI source positions for experiment start-up. *Fusion Engineering and Design*, **86**(6–8) 728–731, October 2011. Proceedings of the 26th Symposium of Fusion Technology (SOFT-26), Porto, Portugal, September 27–October 1, 2010.

[18] Paul McNeely, Marek Barlak, Jürgen Baldzuhn, Sergey Bozhenkov, Michael Drevlak, Grzegorz Gawlik, Bernd Heinemann, Dieter Holtum, Jacek Jagielski, Roland Kairys, Riccardo Nocentini, Rudolf Riedl, Peter Rong, Norbert Rust, Ralf Schroeder, Eckehart Speth, Albrecht Stäbler, Andrzej Turos, and Robert Wolf. Current status of the neutral beam heating system of W7-X. *Fusion Engineering and Design*, **88**(6–8) 1034–1037, October 2013. Proceedings of the 27th Symposium on Fusion Technology (SOFT-27), Liège, Belgium, September 24–28, 2012.

[19] Martin Schmidt, Yuriy Turkin, and Andreas Werner. "Advanced"-δf Monte Carlo simulation of NBI current drive in W7-X. In *31st EPS Conference on Plasma Physics (London, UK)*, volume 28G. European Physical Society, 2004. Poster P-1.200, http://epsppd.epfl.ch/London/pdf/P1_200.pdf.

[20] B. Schweer, J. Ongena, V. Borsuk, D. Birus, S. Bozhenkov, D. Casta no Bardawil, F. Durodié, D. Hartmann, K. P. Hollfeld, P. Kallmeyer, A. Krivska, F. Louche, A. Messiaen, O. Neubauer, G. Offermanns, G. Satheeswaran, M. van Schoor, M. Vervier, R. Wolf, and W7-X Team. Development of an ICRH antenna system at W7-X for plasma heating and wall conditioning. *Fusion Engineering and Design*, **123** 303–308, November 2017. Proceedings of the 29th Symposium on Fusion Technology (SOFT-29), Prague, Czech Republic, September 5–9, 2016.

[21] J. Ongena, A. Messiaen, Ye. O. Kazakov, B. Schweer, I. Stepanov, M. Vervier, M. Berte, K. Crombé, P. Despontin, F. Durodié, G. Jouniaux, A. Krivska, F. Louche, A. Lyssoivan, R. Philips, M. van Schoor, T. Wauters, TEC Team, V. Borsuk, A. Kraemer-Flecken, O. Neubauer, D. Nicolai, G. Satheeswaran, R Schick, TEC Team, D. Casta no Bardawil, K. P. Hollfeld, A. Mauel, G. Offermanns, S. Bozhenkov, A. Dinklage, J. Faustin, D. A. Hartmann, J. P. Kallmeyer, H. Laqua, R. C. Wolf, and W7-X Team. Preparing the ICRH system for the Wendelstein 7-X stellarator.

In *Proceedings of the 27th IAEA Fusion Energy Conference, 22–27 October 2018, Gandhinagar, India*, Vienna, 2019. IAEA. Paper IAEA-CN-258/EX/P8-27.

[22] W. Lotz, P. Merkel, J. Nührenberg, and E. Strumberger. Collisionless α-particle confinement in stellarators. *Plasma Phys. Contr. Fusion*, **34**(6) 1037–1052, June 1992.

[23] Y. Feng, F. Sardei, P. Grigull, K. McCormick, J. Kißlinger, and D. Reiter. Physics of island divertors as highlighted by the example of W7-AS. *Nuclear Fusion*, **46**(8) 807–819, August 2006. http://stacks.iop.org/NF/46/807.

[24] Y. Feng, F. Sardei, P. Grigull, K. McCormick, J. Kißlinger, D. Reiter, and Y. Igitkhanov. Transport in island divertors: physics, 3D modelling and comparison to first experiments on W7-AS. *Plasma Phys. Contr. Fusion*, **44**(5) 611–625, May 2002. http://stacks.iop.org/PPCF/44/611.

[25] Y. Feng, M. Kobayashi, T. Lunt, and D. Reiter. Comparison between stellarator and tokamak divertor transport. *Plasma Phys. Contr. Fusion*, **53**(2) 024009, February 2011. Special section on physics at the stellarator-tokamak interface, http://stacks.iop.org/PPCF/53/024009.

[26] V. Perseo, F. Effenberg, D. Gradic, R. König, O. P. Ford, F. Reimold, D. A. Ennis, O. Schmitz, T. Sunn Pedersen, and W7-X Team. Direct measurements of counter-streaming flows in a low-shear stellarator magnetic island topology. *Nuclear Fusion*, **59**(12) 124003, December 2019.

[27] A. Peacock, H. Greuner, F. Hurd, J. Kißlinger, R. König, B. Mendelevitch, R. Stadler, F. Schauer, R. Tivey, J. Tretter, C. von Sehren, and M. Ye. Progress in the design and development of a test divertor (TDU) for the start of W7-X operation. *Fusion Engineering and Design*, **84**(7–11) 1475–1478, June 2009. Proceedings of the 25th Symposium on Fusion Technology (SOFT-25), Rostock, Germany, 15–19 September 2008.

[28] J. Boscary, A. Peacock, R. Stadler, B. Mendelevitch, H. Tittes, J. Tretter, M. Smirnow, and C. Li. Actively water-cooled plasma facing components of the Wendelstein 7-X stellarator. *Fusion Sci. Tech.*, **64**(2) 263–268, August 2013. Proceedings of the Twentieth Topical Meeting on the Technology of Fusion Energy (TOFE-2012) (Part 1), Nashville, Tennessee, August 27–31, 2012.

[29] M. Jakubowski, A. Ali, P. Drewelow, Y. Gao, K. Hammond, H. Niemann, A. Puig Sitjes, F. Pisano, M. Ślęczka, S. Brezinsek, B. Cannas, M. Endler, R. König, M. Otte, T. S. Pedersen, G. Wurden, D. Zhang, and W7-X Team. 3D heat and particle fluxes in Wendelstein 7-X. In *Proceedings of the 27th Fusion Energy Conference, Ahmedabad,*

India, 22–27 October 2018, Wien, 2018. International Atomic Energy Agency, IAEA. paper EX/P8-16.

[30] R. C. Wolf et al. Major results from the first plasma campaign of the Wendelstein 7-X stellarator. *Nuclear Fusion*, **57**(10) 102020, October 2017.

[31] Thomas Sunn Pedersen, Andreas Dinklage, Yuriy Turkin, Robert Wolf, Sergey Bozhenkov, Joachim Geiger, Golo Fuchert, Hans-Stephan Bosch, Kian Rahbarnia, Henning Thomsen, Ulrich Neuner, Thomas Klinger, Andreas Langenberg, Humberto Trimiño Mora, Petra Kornejew, Jens Knauer, Matthias Hirsch, W7-X Team, and Novimir Pablant. Key results from the first plasma operation phase and outlook for future performance in Wendelstein 7-X. *Phys. Plasmas*, **24**(5) 055503, May 2017.

[32] T. Klinger, A. Alonso, S. Bozhenkov, R. Burhenn, A. Dinklage, G. Fuchert, J. Geiger, O. Grulke, A. Langenberg, M. Hirsch, G. Kocsis, J. Knauer, A. Krämer-Flecken, H. Laqua, S. Lazerson, M. Landreman, H. Maaßberg, S. Marsen, M. Otte, N. Pablant, E. Pasch, K. Rahbarnia, T. Stange, T. Szepesi, H. Thomsen, P. Traverso, J. L. Velasco, T. Wauters, G. Weir, T. Windisch, and The Wendelstein 7-X Team. Performance and properties of the first plasmas of Wendelstein 7-X. *Plasma Phys. Contr. Fusion*, **59**(1) 014018, January 2017. Special Issue featuring the invited talks from the 43rd EPS Conference on Plasma Physics, Leuven, 4–8 July 2016.

[33] J. Baldzuhn, H. Damm, C. D. Beidler, K. McCarthy, N. Panaderio, C. Biedermann, S. A. Bozhenkov, K. J. Brunner, G. Fuchert, Y. Kazakov, M. Beurskens, M. Dibon, J. Geiger, O. Grulke, U. Höfel, T. Klinger, F. Köchl, J. Knauer, G. Kocsis, P. Kornejew, P. T. Lang, A. Langenberg, H. Laqua, N. A. Pablant, E. Pasch, T. S. Pedersen, B. Ploeckl, K. Rahbarnia, G. Schlisio, E. R. Scott, T. Stange, A. von Stechow, T. Szepesi, Y. Turkin, F. Wagner, V. Winters, G. Wurden, D. Zhang, and Wendelstein 7-X Team. Pellet fueling experiments in Wendelstein 7-X. *Plasma Phys. Contr. Fusion*, **61**(9) 095012, September 2019. http://doi.org/10.1088/1361-5687/ab3567.

[34] J. D. Lore, T. Andreeva, J. Boscary, S. Bozhenkov, J. Geiger, J. H. Harris, H. Hoelbe, A. Lumsdaine, D. McGinnis, A. Peacock, and J. Tipton. Design and analysis of divertor scraper elements for the W7-X stellarator. *IEEE Trans. Plasma Sci.*, **42**(3) 539–544, March 2014.

[35] Thomas Sunn Pedersen, Ralf König, Maciej Krychowiak, Marcin Jakubowski, Jürgen Baldzuhn, Sergey Bozhenkov, Golo Fuchert, Andreas Langenberg, Holger Niemann, Daihong Zhang, Kian Rahbarnia, Hans-Stephan Bosch, Yevgen Kazakov, Sebastijan Brezinsek, Yu Gao, Novimir Pablant, and W7-X Team. First results from divertor operation in Wendelstein 7-X. *Plasma Phys. Contr. Fusion*, **61**(1) 014035, January 2019.

[36] R. C. Wolf, A. Alonso, S. Äkäslompolo, J. Baldzuhn, M. Beurskens, C. D. Beidler, C. Biedermann, H.-S. Bosch, S. Bozhenkov, R. Brakel, H. Braune, S. Brezinsek, K.-J. Brunner, H. Damm, A. Dinklage, P. Drewelow, F. Effenberg, Y. Feng, O. Ford, G. Fuchert, Y. Gao, J. Geiger, O. Grulke, N. Harder, D. Hartmann, P. Helander, B. Heinemann, M. Hirsch, U. Höfel, C. Hopf, K. Ida, M. Isobe, M. W. Jakubowski, Y. O. Kazakov, C. Killer, T. Klinger, J. Knauer, R. König, M. Krychowiak, A. Langenberg, H. P. Laqua, S. Lazerson, P. McNeely, S. Marsen, N. Marushchenko, R. Nocentini, K. Ogawa, G. Orozco, M. Osakabe, M. Otte, N. Pablant, E. Pasch, A. Pavone, M. Porkolab, A. Puig Sitjes, K. Rahbarnia, R. Riedl, N. Rust, E. Scott, J. Schilling, R. Schroeder, T. Stange, A. von Stechow, E. Strumberger, T. Sunn Pedersen, J. Svensson, H. Thomsen, Y. Turkin, L. Vano, T. Wauters, G. Wurden, M. Yoshinuma, M. Zanini, D. Zhang, and Wendelstein 7-X Team. Performance of Wendelstein 7-X stellarator plasmas during the first divertor operation phase. *Phys. Plasmas*, **26**(8) 082504, August 2019. Special Collection: Papers from the 60th Annual Meeting of the APS Division of Plasma Physics.

[37] G. Ehrke, B. Mendelevitch, J. Boscary, C. Li, O. Sellmeier, R. Stadler, P. McNeely, F. Schauer, and W7-X Team. Design and manufacturing of the Wendelstein 7-X cryo-vacuum pump. *Fusion Engineering and Design*, **146B** 2757–2760, September 2019. Proceedings of the 30th Symposium on Fusion Technology (SOFT-30), Giardini Naxos, Sicily, Italy, September 16–21, 2018.

[38] L. R. Baylor, S. K. Combs, R. C. Duckworth, M. S. Lyttle, S. J. Meitner, D. A. Rasmussen, and S. Maruyama. Pellet injection technology and its applications on ITER. *IEEE Trans. Plasma Sci.*, **44**(9) 1489–1495, September 2016.

[39] J. Kißlinger and T. Andreeva. Correction possibilities of magnetic field errors in Wendelstein 7-X. *Fusion Engineering and Design*, **74**(1–4) 623–626, November 2005. Proceedings of the 23rd Symposium on Fusion Technology, Venice, Italy, 20–24 September 2004.

[40] T. Andreeva, T. Bräuer, M. Endler, and J. Kißlinger. Compensation of Wendelstein 7-X construction errors by optimisation of module positions. In *38th EPS Conference on Plasma Physics (Strasbourg, 27 June–1 July 2011)*, 2011.

[41] M. Otte, D. Aßmus, C. Biedermann, S. Bozhenkov, T. Bräuer, A. Dudek, J. Geiger, G. Kocsis, S. Lazerson, T. S. Pedersen, F. Schauer, T. Szepesi, B. Standley, and W7-X Team. Setup and initial results from the magnetic flux surface diagnostics at Wendelstein 7-X. *Plasma Phys. Contr. Fusion*, **58**(6) 064003, June 2016. Special issue on the 20th International Stellarator-Heliotron Workshop (Greifswald, Germany, 5–9 October 2015).

[42] S. A. Bozhenkov, S. Lazerson, M. Otte, D. A. Gates, T. Sunn Pedersen, and R. C. Wolf. Methods for measuring 1/1 error field in Wendelstein 7-X stellarator. *Nuclear Fusion*, **56**(7) 076002, July 2016.

[43] Samuel A. Lazerson, Matthias Otte, Sergey Bozhenkov, Christoph Biedermann, Thomas Sunn Pedersen, and W7-X Team. First measurements of error fields on W7-X using flux surface mapping. *Nuclear Fusion*, **56**(10) 106005, October 2016.

[44] T. Sunn Pedersen, M. Otte, S. Lazerson, P. Helander, S. Bozhenkov, C. Biedermann, T. Klinger, R. C. Wolf, H.-S. Bosch, and Wendelstein 7-X Team. Confirmation of the topology of the Wendelstein 7-X magnetic field to better than 1:100,000. *Nat. Commun.*, **7** 13493, 30 November 2016.

[45] S. A. Bozhenkov, M. W. Jakubowski, H. Niemann, S. A. Lazerson, G. A. Wurden, C. Biedermann, G. Kocsis, R. König, F. Pisano, L. Stephey, T. Szepesi, U. Wenzel, T. S. Pedersen, R. C. Wolf, and W7-X Team. Effect of error field correction coils on W7-X limiter loads. *Nuclear Fusion*, **57**(12) 126030, December 2017.

[46] Samuel A. Lazerson, Matthias Otte, Marcin Jakubowski, Ben Israeli, Glen A. Wurden, Uwe Wenzel, Tamara Andreeva, Sergey Bozhenkov, Christoph Biedermann, Gábor Kocsis, Tamás Szepesi, Joachim Geiger, Thomas Sunn Pedersen, David Gates, and W7-X Team. Error field measurement, correction and heat flux balancing on Wendelstein 7-X. *Nuclear Fusion*, **57**(4) 046026, April 2017.

[47] Samuel A. Lazerson, Sergey Bozhenkov, Ben Israeli, Matthias Otte, Holger Niemann, Victor Bykov, Michael Endler, Tamara Andreeva, Adnan Ali, Peter Drewelow, Marcin Jakubowski, Aleix Puig Sitjes, Fabio Pisano, Barbara Cannas, and W7-X Team. Error fields in the Wendelstein 7-X stellarator. *Plasma Phys. Contr. Fusion*, **60**(12) 124002, December 2018. Special Issue on the 21st International Stellarator-Heliotron Workshop, https://iopscience.iop.org/article/10.1088/1361-6587/aae96b.

[48] S. A. Bozhenkov, M. Otte, C. Biedermann, M. Jakubowski, S. A. Lazerson, T. Sunn Pedersen, R. C. Wolf, and W7-X Team. Measurements and correction of the 1/1 error field in Wendelstein 7-X. *Nuclear Fusion*, **59**(2) 026004, February 2019.

[49] K. C. Hammond, Y. Gao, M. Jakubowski, C. Killer, H. Niemann, L. Rudischhauser, A. Ali, T. Andreeva, B. D. Blackwell, K. J. Brunner, B. Cannas, P. Drewelow, P. Drews, M. Endler, Y. Feng, J. Geiger, O. Grulke, J. Knauer, S. Klose, S. Lazerson, M. Otte, F. Pisano, U. Neuner, A. Puig Sitjes, K. Rahbarnia, J. Schilling, H. Thomsen, G. A. Wurden, and W7-X Team. Drift effects on W7-X divertor heat and particle fluxes. *Plasma Phys. Contr. Fusion*, **61**(12) 125001, December 2019.

[50] T. Andreeva, J. A. Alonso, S. Bozhenkov, C. Brandt, M. Endler, G. Fuchert, J. Geiger, M. Grahl, T. Klinger, M. Krychowiak, A. Langenberg, S. Lazerson, U. Neuner, K. Rahbarnia, N. Pablant, A. Pavone, J. Schilling, J. Schmitt, H. Thomsen, Y. Turkin, and W7-X Team. Equilibrium evaluation for Wendelstein 7-X experiment programs in the first divertor phase. *Fusion Engineering and Design*, **146A** 299–302, September 2019. Proceedings of the 30th Symposium on Fusion Technology (SOFT-30), Giardini Naxos, Sicily, Italy, September 16–21, 2018.

[51] U. Neuner, K. Rahbarnia, C. D. Beidler, A. Dinklage, Y. Turkin, T. Stange, T. Andreeva, J. Schilling, H. Thomsen, M. N. A. Beurskens, S. A. Bozhenkov, K. J. Brunner, H. Damm, G. Fuchert, J. Geiger, U. Hergenhahn, U. Höfel, J. P. Knauer, M. Krychowiak, S. Kwak, A. Langenberg, N. A. Pablant, E. Pasch, A. Pavone, E. R. Scott, J. Svensson, H. Trimino Mora, and Wendelstein 7-X team. Measurements of the parameter dependencies of the bootstrap current in the W7-X stellarator. 2021. DOI: 10.1088/1741-4326/abd61a.

[52] J. Geiger, C. D. Beidler, M. Drevlak, H. Maaßberg, C. Nührenberg, Y. Suzuki, and Yu. Turkin. Effects of net currents on the magnetic configuration of W7-X. *Contrib. Plasma Phys.*, **50**(8) 770–774, August 2010. Special Issue: Proceedings of 17th International Stellarator/Heliotron Workshop, October 12–16, 2009, Princeton Plasma Physics Laboratory (PPPL), Princeton, New Jersey, USA (Part II).

[53] H. Hölbe, T. Sunn Pedersen, J. Geiger, S. Bozhenkov, R. König, Y. Feng, J. Lore, A. Lumsdaine, and Wendelstein 7-X Team. Access to edge scenarios for testing a scraper element in early operation phases of Wendelstein 7-X. *Nuclear Fusion*, **56**(2) 026015, February 2016.

[54] Yu Gao, Joachim Geiger, Marcin W. Jakubowski, Peter Drewelow, Michael Endler, Kian Rahbarnia, Sergey Bozhenkov, Matthias Otte, Yasuhiro Suzuki, Yuhe Feng, Holger Niemann, Fabio Pisano, Adnan Ali, Aleix Puig Sitjes, Marco Zanini, Heinrich Laqua, Torsten Stange, Stefan Marsen, Tamas Szepesi, Daihong Zhang, Carsten Killer, Kenneth Hammond, Samuel Lazerson, Barbara Cannas, Henning Thomsen, Tamara Andreeva, Ulrich Neuner, Jonathan Schilling, Alexander Knieps, Michael Rack, Yunfeng Liang, and W7-X Team. Effects of toroidal plasma current on divertor power depositions on Wendelstein 7-X. *Nuclear Fusion*, **59**(10) 106015, October 2019.

[55] R. C. Wolf, S. Bozhenkov, A. Dinklage, G. Fuchert, Y. O. Kazakov, H. P. Laqua, S. Marsen, N. B. Marushchenko, T. Stange, M. Zanini, I. Abramovic, A. Alonso, J. Baldzuhn, M. Beurskens, C. D. Beidler, H. Braune, K. J. Brunner, N. Chaudhary, H. Damm, P. Drewelow, G. Gantenbein, Yu Gao, J. Geiger, M. Hirsch, U. Höfel, M. Jakubowski, J. Jelonnek, T. Jensen, W. Kasparek, J. Knauer, S. B. Korsholm, A. Langenberg, C. Lechte, F. Leipold, H. Trimino Mora, U. Neuner, S. K. Nielsen,

D. Moseev, H. Oosterbeek, N. Pablant, E. Pasch, B. Plaum, T. Sunn Pedersen, A. Puig Sitjes, K. Rahbarnia, J. Rasmussen, M. Salewski, J. Schilling, E. Scott, M. Stejner, H. Thomsen, M. Thumm, Y. Turkin, F. Wilde, and Wendelstein 7-X Team. Electron-cyclotron-resonance heating in Wendelstein 7-X: A versatile heating and current-drive method and a tool for in-depth physics studies. *Plasma Phys. Contr. Fusion*, **61**(1) 014037, January 2019.

[56] Heinrich Peter Laqua and W7-X Team. Steady state ECRH operation at the W7-X stellarator, 2021. Accepted (Proceedings of the 29th International Toki Conference (ITC-29), Ceratopia Toki, Toki City, Gifu, Japan, October 27–30, 2020).

[57] C. D. Beidler, H. M. Smith, A. Alonso, T. Andreeva, J. Baldzuhn, M. N. A. Beurskens, M. Borchardt, S. A. Bozhenkov, K. J. Brunner, H. Damm, M. Drevlak, O. P. Ford, G. Fuchert, J. Geiger, P. Helander, M. Hirsch, U. Höfel, Y. Kazakov, R. Kleiber, M. Krychowiak, A. Langenberg, H. P. Laqua, U. Neuner, N. A. Pablant, E. Pasch, A. Pavone, T. Sunn Pedersen, K. Rahbarnia, J. Schilling, E. R. Scott, T. Stange, H. Thomsen, Y. Turkin, F. Warmer, R. C. Wolf, D. Zhang, and W7-X Team. Successful reduction of neoclassical energy transport in Wendelstein 7-X. *Nature*, 2021. Submitted.

[58] E. M. Edlund, M. Porkolab, Z. Huang, O. Grulke, L.-G. Böttger, C. von Sehren, and A. von Stechow. Overview of the Wendelstein 7-X phase contrast imaging diagnostic. *Review of Scientific Instruments*, **89**(10) 10E105, October 2018. Proceedings of the 22nd Topical Conference on High-Temperature Plasma Diagnostics, San Diego, CA, USA, 16–19 April 2018.

[59] A. von Stechow, O. Grulke, Th. Wegner, J. H. E. Proll, J. A. Alcusón, H. M. Smith, J. Baldzuhn, C. D. Beidler, M. N. A. Beurskens, S. A. Bozhenkov, E. Edlund, B. Geiger, Z. Huang, O. P. Ford, G. Fuchert, A. Langenberg, N. Pablant, E. Pasch, M. Porkolab, K. Rahbarnia, J. Schilling, E. R. Scott, H. Thomsen, L. Vanó, G. Weir, and W7-X Team. Suppression of core turbulence by profile shaping in Wendelstein 7-X. 2021. Submitted to Phys. Rev. Letters.

[60] J. H. E. Proll, P. Helander, J. W. Connor, and G. G. Plunk. Resilience of quasi-isodynamic stellarators against trapped-particle instabilities. *Physical Review Letters*, **108**(24) 245002, 15 June 2012.

[61] J. A. Alcusón, P. Xanthopoulos, G. G. Plunk, P. Helander, F. Wilms, Y. Turkin, A. von Stechow, and O. Grulke. Suppression of electrostatic microinstabilities in maximum-J stellarators. *Plasma Phys. Contr. Fusion*, **62**(3) 035005, March 2020.

[62] P. Xanthopoulos, S. A. Bozhenkov, M. N. Beurskens, H. M. Smith, G. G. Plunk, P. Helander, C. D. Beidler, J. A. Alcusón, A. Alonso, A. Dinklage, O. Ford, G. Fuch-

ert, J. Geiger, J. H. E. Proll, M. J. Pueschel, Y. Turkin, F. Warmer, and W7-X Team. Turbulence mechansims of enhanced performance stellarator plasmas. *Physical Review Letters*, **125**(7) 075001, 14 August 2020.

[63] E. Wang, S. Brezinsek, S. Sereda, B. Buttenschön, T. Barbui, C. P. Dhard, M. Endler, O. Ford, E. Flom, K. C. Hammond, M. Jakubowski, M. Krychowiak, P. Kornejew, R. König, Y. Liang, M. Mayer, D. Naujoks, O. Neubauer, J. Oelmann, M. Rasinski, V. R. Winters, A. Goriaev, T. Wauters, Y. Wei, D. Zhang, and W7-X Team. Impurity sources and fluxes in W7-X: from the plasma-facing components to the edge layer. *Physica Scripta*, **2020**(T171) 014040, 4 March 2020.

[64] S. Sereda, S. Brezinsek, E. Wang, T. Barbui R. Brakel, B. Buttenschön, A. Goriaev, U. Hergenhahn, U. Höfel, M. Jakubowski, A. Knieps, R. König, M. Krychowiak, S. Kwak, Y. Liang, D. Naujoks, A. Pavone, M. Rasinski, L. Rudischhauser, M. Ślęczka, J. Svensson, H. Viebke, T. Wauters, Y. Wei, V. Winters, D. Zhang, and W7-X Team. Impact of boronizsations on impurity sources and performance in Wendelstein 7-X. *Nuclear Fusion*, **60**(8) 086007, August 2020.

[65] S. Sudo, Y. Takeiri, H. Zushi, F. Sano, K. Itoh, K. Kondo, and A. Iiyoshi. Scalings of energy confinement and density limit in stellarator/heliotron devices. *Nuclear Fusion*, **30**(1) 11–21, January 1990.

[66] G. Fuchert, K. J. Brunner, K. Rahbarnia, T. Stange, D. Zhang, J. Baldzuhn, S. A. Bozhenkov, C. D. Beidler, M. N. A. Beurskens, S. Brezinsek, R. Burhenn, H. Damm, A. Dinklage, Y. Feng, P. Hacker, M. Hirsch, Y. Kazakov, J. Knauer, A. Langenberg, H. P. Laqua, S. Lazerson, N. A. Pablant, E. Pasch, F. Reimold, T. Sunn Pedersen, E. R. Scott, F. Warmer, V. R. Winters, R. C. Wolf, and W7-X Team. Increasing the density in Wendelstein 7-X: benefits and limitations. *Nuclear Fusion*, **60**(3) 036020, March 2020.

[67] Oliver Schmitz, Y. Feng, M. Jakubowski, R. König, M. Krychowiak, M. Otte, F. Reimold, T. Barbui, C. Biedermann, S. Bozhenkov, S. Brezinsek, B. Buttenschön, K. J. Brunner, P. Drewelow, F. Effenberg, E. Flom, H. Frerichs, O. Ford, G. Fuchert, Y. Gao, D. Gradic, O. Grulke, K. C. Hammond, U. Hergenhahn, U. Höfel, J. Knauer, P. Kornejew, T. Kremeyer, H. Niemann, E. Pasch, A. Pavone, V. Perseo, L. Rudischhauser, G. Schlisio, T. Sunn Pedersen, U. Wenzel, V. Winters, G. A. Wurden, D. Zhang, and W7-X Team. Stable heat and particle flux detachment with efficient particle exhaust in the island divertor of Wendelstein 7-X. *Nuclear Fusion*, **61**(1) 016026, January 2021.

[68] O. Grulke and Wendelstein 7-X Team. Wendelstein 7-X towards high-density, long-pulse operation, 2019. Plenary presentation I3.008, at 46th European Physical Society Conference on Plasma Physics, 8–12 July 2019, Milano, Italy.

[69] A. Puig Sitjes, M. Jakubowski, J. Fellinger, P. Drewelow, Y. Gao, H. Niemann, T. S. Pedersen, R. König, D. Naujoks, A. Winter, H. Laqua, S. Dumke, T. Bluhm, K. Brandt, V. Moncada, C. Belafdil, R. Mitteau, M. H. Aumeunier, F. Pisano, E. Aymerich, B. Cannas, G. Kocsis, T. Szepesi, G. Cseh, T. Szabolics, J. R. Casas, J. R. Morros, P. Salembier, R. Clemente, M. Cobos, I. Caminal, A. Palacios, A. Moreno, S. Quiceno, and W7-X Team. Strategy for the real-time detection of thermal events on the plasma facing components of Wendelstein 7-X. Poster P3.73 on 31st Symposium on Fusion Technology (SOFT2020), 20–25 September 2020, virtual edition.

[70] K. A. Avramidis, Z. C. Ioannidis, G. Aiello, P. Bénin, I. Chelis, A. Dinklage, G. Gantenbein, S. Illy, J. Jelonnek, J. Jin, H. P. Laqua, A. Leggieri, F. Legrand, A. Marek, S. Marsen, I. Gr. Pagonakis, T. Ruess, T. Rzesnicki, T. Scherer, D. Strauss, M. Thumm, I. Tigelis, D. Wagner, J. Weggen, R. C. Wolf, and Wendelstein 7-X Tean. Towards a 1.5 MW, 140 GHz gyrotron for the upgraded ECRH system at W7-X. Poster P2.37 on 31st Symposium on Fusion Technology (SOFT2020), 20–25 September 2020, virtual edition.

[71] G. Aiello, K. A. Avramidis, G. Gantenbein, J. Jelonnek, J. Jin, H. P. Laqua, A. Meier, T. Scherer, D. Strauss, and M. Thumm. Design validation of the gyrotron diamond output window for the upgrade of the ECRH system at W7-X. Poster P1.24 on 31st Symposium on Fusion Technology (SOFT2020), 20–25 September 2020, virtual edition.

[72] P. McNeely, S. Degenkolbe, O. P. Ford, D. A. Hartmann, B. Heinemann, T. Richert, R. Riedl, R. Schroeder, P. van Eeten, and W7-X Team. A safety system for fast beam termination on W7-X. Poster P2.62 on 31st Symposium on Fusion Technology (SOFT2020), 20–25 September 2020, virtual edition.

[73] D. A. Castaño Bardawil, B. Schweer, J. Ongena, W. Behr, K. Crombé, G. Czymek, X. Han, D. Hartmann, K. P. Hollfeld, J. P. Kallmeyer, A. Krämer-Flecken, Ch. Linsmeier, O. Neubauer, D. Nicolai, G. Offermanns, G. Satheeswaran, I. Stepanov, M. Van Schoor, M. Vervier, and R. Wolf. Design improvements, assembly and testing of the ICRH antenna for W7-X. Poster P1.91 on 31st Symposium on Fusion Technology (SOFT2020), 20–25 September 2020, virtual edition.

[74] E. Pasch, M. N. A. Beurskens, S. A. Bozhenkov, G. Fuchert, R. C. Wolf, and W7-X Team. Dual-laser wavelength Thomson scattering at Wendelstein 7-X. *Review of Scientific Instruments*, **89**(10) 10C115, October 2018. Proceedings of the 22nd Topical Conference on High-Temperature Plasma Diagnostics, San Diego, CA, USA, 16–19 April 2018.

[75] L. Rudischhauser, M. Endler, U. Höfel, K. C. Hammond, J. P. Kallmeyer, B. D. Blackwell, and Wendelstein 7-X Team. The Langmuir probe system in the Wendelstein 7-X test divertor. *Review of Scientific Instruments*, **91**(6) 063505, June 2020.

[76] M. Hubeny, D. Höschen, O. Neubauer, R. Hoek, G. Czymek, D. Naujoks, D. Hathiramani, C. Castaño Bardawil, B. Unterberg, R. König, S. Brezinsek, Ch. Linsmeier, and W7-X Team. Progress on MATEO probe heads and observation system. Poster P4.29 on 31st Symposium on Fusion Technology (SOFT2020), 20–25 September 2020, virtual edition.

[77] D. Höschen, M. Hubeny, G. Czymek, O. Neubauer, D. Naujoks, D. Hathiramani, D. Castaño Bardawil, B. Unterberg, R. König, S. Brezinsek, Ch. Linsmeier, and W7-X Team. Design aspects of the MATEO manipulator at Wendelstein 7-X. Poster P4.30 on 31st Symposium on Fusion Technology (SOFT2020), 20–25 September 2020, virtual edition.

[78] S. J. Zweben, J. L. Terry, D. P. Stotler, and R. J. Maqueda. Gas puff imaging diagnostics of edge plasma turbulence in magnetic fusion devices (invited review article). *Review of Scientific Instruments*, **88**(4) 041101, April 2017.

[79] Samuel A. Lazerson, Robert Ellis, Chris Freeman, Jessica Ilagan, Tianyao Wang, Lin Shao, Nicole Allen, David Gates, and Hutch Neilson. Development of a Faraday cup fast ion loss detector for keV beam ions. *Review of Scientific Instruments*, **90**(9) 093504, September 2019.

[80] P. Sinha, D. Böckenhoff, M. Endler, J. Geiger, H. Hölbe, H. M. Smith, T. S. Pedersen, Y. Turkin, and W7-X Team. Scenario with combined density and heating control to reduce the impact of the bootstrap current in Wendelstein 7-X. *Nuclear Fusion*, **59**(12) 126012, December 2019.

[81] Mitsuri Kikuchi and Masafumi Azumi. *Frontiers in Fusion Research II (Introduction to Modern Tokamak Physics)*. Springer, Cham, Heidelberg, New York, Dordrecht, London, 2015.

[82] Gaetano Bongiovì, André Häußler, Salvatore Giambrone, Ilenia Catanzaro, Ruggero Forte, Guangming Zhou, Pietro Alessandro Di Maio, and W7-X Team. Structural assessment of a whole toroidal sector of the HELIAS 5-B breeding blanket. Poster P2.75 on 31st Symposium on Fusion Technology (SOFT2020), 20–25 September 2020, virtual edition.

[83] J. Lion, F. Warmer, and R. C. Wolf. Modelling a general class of stellarators in the systems code PROCESS. Poster P1.166 on 31st Symposium on Fusion Technology (SOFT2020), 20–25 September 2020, virtual edition.

[84] F. Warmer. A strategy to accelerate stellerator engineering in preparation of a next-step device. Poster P2.52 on 31st Symposium on Fusion Technology (SOFT2020), 20–25 September 2020, virtual edition.

[85] R. König, J. Baldzuhn, W. Biel, C. Biedermann, R. Burhenn, S. Bozhenkov, J. Cantarini, H. Dreier, M. Endler, H.-J. Hartfuss, D. Hildebrandt, M. Hirsch, M. Jakubowski, R. Jimenez-Gomez, G. Kocsis, P. Kornejew, M. Krychowiak, H. P. Laqua, M. Laux, J. W. Oosterbeek, E. Pasch, T. Richert, W. Schneider, B. Schweer, J. Svensson, H. Thomsen, A. Weller, A. Werner, R. Wolf, D. Zhang, and S. Zoletnik. Diagnostics design for steady-state operation of the Wendelstein 7-X stellarator. *Review of Scientific Instruments*, **81**(10) 10E133, October 2010. Proceedings of the 18th Topical Conference on High-Temperature Plasma Diagnostics, Wildwood, NJ, USA, 16–20 May 2010.

[86] R. König, J. Baldzuhn, C. Biedermann, R. Burhenn, S. Bozhenkov, A. Cardella, M. Endler, H.-J. Hartfuss, D. Hathiramani, D. Hildebrandt, M. Hirsch, M. Jakubowski, G. Kocsis, P. Kornejew, M. Krychowiak, H. P. Laqua, M. Laux, J. W. Oosterbeek, E. Pasch, T. Richert, W. Schneider, T. Sunn Pedersen, H. Thomsen, A. Weller, A. Werner, R. Wolf, D. Zhang, and S. Zoletnik. Diagnostics development for quasi-steady-state operation of the Wendelstein 7-X stellarator (invited). *Review of Scientific Instruments*, **83**(10) 10D730, October 2012. Proceedings of the 19th Topical Conference on High-Temperature Plasma Diagnostics, Monterey, CA, USA, 6–10 May 2012.

[87] Dag Hathiramani, Roland Binder, Rudolf Brakel, Torsten Broszat, Bertram Brucker, Antonino Cardella, Michael Endler, Klaus Grosser, Matthias Hirsch, Heinrich Laqua, and Stefan Thiel. Microwave stray radiation: Measures for steady state diagnostics at Wendelstein 7-X. *Fusion Engineering and Design*, **88**(6–8) 1232–1235, October 2013. Proceedings of the 27th Symposium on Fusion Technology (SOFT-27), Liège, Belgium, 24–28 September 2012.

[88] M. Endler, B. Brucker, V. Bykov, A. Cardella, A. Carls, F. Dobmeier, A. Dudek, J. Fellinger, J. Geiger, K. Grosser, O. Grulke, D. Hartmann, D. Hathiramani, K. Höchel, M. Köppen, R. Laube, U. Neuner, X. Peng, K. Rahbarnia, K. Rummel, T. Sieber, S. Thiel, A. Vorköper, A. Werner, T. Windisch, and M. Y. Ye. Engineering design for the magnetic diagnostics of Wendelstein 7-X. *Fusion Engineering and Design*, **100** 468–494, November 2015.

[89] Uwe Wenzel, Georg Schlisio, Matthias Mulsow, Thomas Sunn Pedersen, Martin Singer, Mirko Marquardt, Dirk Pilopp, and Nils Rüter. Performance of new crystal cathode pressure gauges for long-pulse operation in the Wendelstein 7-X stellarator. *Review of Scientific Instruments*, **90**(12) 123507, December 2019.

[90] Heike Laqua, Helmut Niedermeyer, and Jörg Schacht. Control system of Wendelstein 7-X experiment. *Fusion Engineering and Design*, **66–68** 669–673, September 2003. Proceedings of the 22nd Symposium on Fusion Technology, Helsinki, Finland, 9–13 September 2002.

[91] Heike Laqua, Torsten Bluhm, Peter Heimann, Christine Hennig, Hugo Kroiss, Jon G. Krom, Georg Kühner, Marc Lewerentz, Josef Maier, Jörg Schacht, Anett Spring, and Andreas Werner. Resource checking and event handling within the W7-X segment control framework. *Fusion Engineering and Design*, **87**(12) 1958–1960, December 2012. Proceedings of the 8th IAEA Technical Meeting on Control, Data Acquisition, and Remote Participation for Fusion Research, San Francisco, CA, USA, 20–24 June 2011.

[92] T. Bluhm, P. Heimann, Ch. Hennig, G. Kühner, H. Kroiss, J. Krom, H. Laqua, M. Lewerentz, J. Maier, H. Riemann, J. Schacht, A. Spring, A. Werner, and M. Zilker. Wendelstein 7-X's CoDaStation — a modular application for scientific data acquisition. *Fusion Engineering and Design*, **89**(5) 658–662, May 2014. Proceedings of the 9th IAEA Technical Meeting on Control, Data Acquisition, and Remote Participation for Fusion Research, Hefei, China, 6–10 May 2013.

[93] Christine Hennig, Josef Maier, Martin Grün, Jon Krom, Torsten Bluhm, Michael Grahl, Peter Heimann, Heike Riemann, Heike Laqua, Marc Lewerentz, Anett Spring, and Andreas Werner. ArchiveDB—scientific and technical data archive for Wendelstein 7-X. *Fusion Engineering and Design*, **112** 984–990, 15 November 2016. Proceedings of the 10th IAEA Technical Meeting on Control, Data Acquisition and Remote Participation for Fusion Research, Ahmedabad, India, 20–24 April 2015.

[94] Jörg Schacht, Helmut Niedermeyer, Christian Wiencke, Jens Hildebrandt, and Andreas Wassatsch. A trigger-time-event system for the W7-X experiment. *Fusion Engineering and Design*, **60**(3) 373–379, June 2002. Proceedings of the 3rd IAEA Technical Committee Meeting on Control, Data Acquisition, and Remote Participation for Fusion Research, Padova, Italy, 16–19 July 2001.